The renal cortical collecting duct: a secreting epithelium?

Luciana Morla, Alain Doucet, Christine Lamouroux, Gilles Crambert, Aurélie Edwards

To cite this version:

Luciana Morla, Alain Doucet, Christine Lamouroux, Gilles Crambert, Aurélie Edwards. The renal cortical collecting duct: a secreting epithelium?. The Journal of Physiology, 2016, 594 (20), pp.5991 - 6008. 10.1113/JP272877 . hal-01411560

HAL Id: hal-01411560
https://hal.sorbonne-universite.fr/hal-01411560

Submitted on 7 Dec 2016

HAL is a multi-disciplinary open access archive for the deposit and dissemination of scientific research documents, whether they are published or not. The documents may come from teaching and research institutions in France or abroad, or from public or private research centers.

L'archive ouverte pluridisciplinaire **HAL**, est destinée au dépôt et à la diffusion de documents scientifiques de niveau recherche, publiés ou non, émanant des établissements d'enseignement et de recherche français ou étrangers, des laboratoires publics ou privés.

The Renal Cortical Collecting Duct: a Secreting Epithelium?

Luciana Morla[1], Alain Doucet[1], Christine Lamouroux[1], Gilles Crambert[1*], Aurélie Edwards[1*]

[1]Sorbonne Universités, UPMC Univ Paris 06, INSERM, Université Paris Descartes, Sorbonne Paris Cité, UMR_S 1138, CNRS, ERL 8228, Centre de Recherche des Cordeliers, F-75006, Paris, France

*co-last authors.

Running title: H/K-ATPase-mediated Sodium Secretion in the Mouse Collecting Duct

Keywords: sodium; collecting duct; mathematical model.

Corresponding author:

Aurélie Edwards

UMRS 1138, Equipe 3

Centre de Recherche des Cordeliers

15 rue de l'Ecole de Médecine

75006 Paris

France

Tel: (33) 144 275 099

Email address: aurelie.edwards@crc.jussieu.fr

Key point summary

- The cortical collecting duct (CCD) plays an essential role in sodium homeostasis by fine-tuning the amount of sodium that is excreted in the urine.
- Ex vivo, the microperfused CCD reabsorbs sodium in the absence of lumen-to-bath concentration gradients.
- In this study, we show that in the presence of physiological lumen-to-bath concentration gradients, and in the absence of endocrine, paracrine, and neural regulation, the mouse CCD secretes sodium, which represents a paradigm shift.
- This secretion occurs via the paracellular route, as well as a transcellular pathway which is energized by apical H^+/K^+-ATPase type 2 pumps operating as Na^+/K^+ exchangers.
- The newly identified transcellular secretory pathway represents a physiological target for the regulation of sodium handling and for anti-hypertensive therapeutic agents.

ABSTRACT

In vitro microperfusion experiments have demonstrated that cortical collecting ducts (CCDs) reabsorb sodium via principal and type B intercalated cells under sodium-depleted conditions and thereby contribute to sodium and blood pressure homeostasis. However, these experiments were performed in the absence of the transepithelial ion concentration gradients that prevail *in vivo* and determine paracellular transport. This study aimed to characterize Na^+, K^+, and Cl^- fluxes in the mouse CCD in the presence of physiological transepithelial concentration gradients. For this purpose we combined *in vitro* measurements of ion fluxes across microperfused CCDs of sodium-depleted mice with the predictions of a mathematical model. When NaCl transport was inhibited in all cells, CCDs secreted Na^+ and reabsorbed K^+; Cl^- transport was negligible. Removing inhibitors of type A and B intercalated cells increased Na^+ secretion in wild-type (WT) mice but not in H^+/K^+-ATPase type 2 (HKA2) knock-out mice. Further inhibition of basolateral NaCl entry via the Na^+-K^+-$2Cl^-$ cotransporter in type A intercalated cells reduced Na^+ secretion in WT mice to the levels observed in $HKA2^{-/-}$ mice . With no inhibitors, WT mouse CCDs still secreted Na^+ and reabsorbed K^+. *In vivo*, $HKA2^{-/-}$ mice excreted less Na^+ than WT mice after switching to a high-salt diet. Altogether our results indicate that type A intercalated cells secrete Na^+ via basolateral Na^+-K^+-$2Cl^-$ cotransporters in tandem with apical HKA2 pumps. They also suggest that the CCD can mediate overall Na^+ secretion, and that its ability to reabsorb NaCl *in vivo* depends on the presence of acute regulatory factors.

Word count: 249.

ABBREVIATION LIST

CCD, cortical collecting duct; ENaC, epithelial Na^+ channel; HCTZ, hydrochlorothiazide; HKA2, H^+/K^+-ATPase type 2; IMCD, inner medullary collecting duct; NDCBE, Na^+-driven Cl^-/HCO_3^- exchanger; ROMK, renal outer medullary K^+ channel; ΔV_{te}, transepithelial electric potential difference.

INTRODUCTION

The urinary excretion of sodium, potassium, and chloride is fine-tuned in the aldosterone-sensitive distal nephron, which consists of the distal convoluted tubule, the connecting tubule, and the collecting duct. Results based on the microperfusion technique have shown that the cortical collecting duct (CCD) mediates NaCl reabsorption in response to aldosterone or sodium depletion. The CCD epithelium consists of principal cells and intercalated cells; the latter are subdivided into type A, type B, and non-A non-B. Until recently, sodium reabsorption in the CCD was thought to be mediated exclusively by principal cells, via the amiloride-sensitive epithelial Na^+ channel (ENaC) on the apical side and Na^+/K^+ ATPase on the basolateral side. In 1990, Terada and Knepper identified an additional, thiazide-sensitive NaCl transport pathway in the rat CCD (Terada & Knepper, 1990). Several groups subsequently characterized this pathway in the mouse CCD. Wall and coworkers first showed that Cl^- reabsorption is abolished in mice lacking the apical Cl^-/HCO_3^- exchanger pendrin (slc26a4) (Wall *et al.*, 2004). Eladari and colleagues then demonstrated that type B intercalated cells can mediate NaCl reabsorption under the concerted action of several transporters, including pendrin, the apical Na^+-driven Cl^-/HCO_3^- exchanger NDCBE (slc4a8), and the basolateral Na^+/HCO_3^- cotransporter AE4 (Slc4a9)(Leviel *et al.*, 2010).They also showed that this NaCl reabsorption is energized by the basolateral H-ATPase (Chambrey *et al.*, 2013).

In addition, Wall and coworkers recently showed that following aldosterone administration, type A intercalated cells in the CCD of sodium-replete mice express the bumetanide-sensitive Na^+-K^+-$2Cl^-$ cotransporter 1 NKCC1 (slc12a2) in the basolateral region. They found, moreover, that ENaC inhibition stimulates Cl^- secretion through a NKCC1-dependent mechanism (Pech *et al.*, 2012). Since NKCC1 carries one Na^+ ion and one K^+ ion together with 2 Cl^- ions into the cell, type A cells could also mediate Na^+ secretion across the CCD, via NKCC1 on the basolateral side and to-be-determined Na^+ transporters on the apical side. In fact, bumetanide-sensitive Na^+ secretion was observed in the outer medullary collecting ducts of deoxycorticosterone pivalate (DOCP)-treated rats that were perfused *in vitro* (Wall & Fischer, 2002), but the underlying pathways were not elucidated.

Since CCDs are not accessible to *in vivo* micropuncture and microperfusion studies, our understanding of their transport function derives from *in vitro* microperfusion experiments. However, ion fluxes across the CCD are usually measured under symmetric conditions, that is, with identical solutions in the perfusion solution and the bath, whereas *in vivo* the composition of the tubular fluid entering the CCD differs significantly from that of the surrounding interstitium. The luminal concentration of Na^+ and Cl^- in the late superficial distal tubule is 0.2 to 0.5 times that in plasma; conversely, the concentration of K^+ is 2-4 times greater in the lumen than in the interstitium (Elalouf *et al.*, 1984; Beck *et al.*, 1988). The luminal concentration of HCO_3^- has been reported as 5 mM (Buerkert *et al.*, 1983). In the presence of these transepithelial concentration gradients, the paracellular pathway should mediate Na^+ secretion, thereby counterbalancing, at least partly, Na^+ reabsorption across principal and type B cells.

The objective of the present study was to determine the net direction of NaCl transport across the CCD under asymmetric conditions as encountered *in vivo*, and to characterize the contribution of each pathway to overall fluxes. For this purpose, we combined measurements of ion fluxes across microperfused cortical collecting ducts with the predictions of a mathematical model of transepithelial transport across the CCD.

METHODS

Ethical approval

Experimental protocols were approved by the Darwin's Ethic Committee and the French Ministère de la Recherche (Agreement # 2289.01).

Experimental procedures

All experiments were performed on male 8-10 week-old mice. A colony of H^+/K^+-ATPase type 2 (HKA2) knockout mice (C57BL/6J background) was obtained from P. Meneton (Meneton *et al.*, 1998). Control (WT) mice were either commercial C57BL/6J mice (Charles River) or littermate homozygous HKA2$^{+/+}$ mice; there was no difference between these mice and their results were pooled. All animals were fed a Na^+-depleted diet (containing 0.11 g of Na^+ per kg) for 2 weeks before the microperfusion experiments.

Microperfusion studies. Mice were killed by cervical dislocation and their right kidney was removed. CCDs were microdissected from cortico-medullary rays and microperfused under asymmetrical conditions. The bath contained 118 mM NaCl, 23 mM $NaHCO_3$, 1.2 mM $MgSO_4$, 2 mM K_2HPO_4, 2 mM calcium lactate, 1 mM sodium citrate, 5.5 mM glucose, and 12 mM creatinine, at pH 7.4. The perfused solution contained 74 mM NaCl, 1 mM KCl, 2 mM K_2HPO_4, 5 mM K-gluconate, 5 mM $KHCO_3$, 1.2 mM $MgSO_4$, 2 mM calcium lactate, 1 mM sodium citrate, 5.5 mM glucose, and 12 mM creatinine, at pH 7.04. The bath and perfusate were continuously gassed with 95% O_2/5% CO_2 at 37°C. The transepithelial voltage difference (ΔV_{te}) was measured via microelectrodes connected through an Ag/AgCl half-cell to an electrometer. Measurements were performed during the first 90 minutes of perfusion. During 4 periods of 15 minutes each, 30–35 nl of fluid were collected. The collection volume was determined under water-saturated mineral oil with calibrated volumetric pipettes. Concentrations of Na^+, K^+ and creatinine were determined by HPLC using 26 nl of collected fluid. Concentrations of Cl^- were measured by microcoulometry on 2 to 3 nl of collected fluid. For each collection period, the flux of ion X per unit length of tubule (J_X) was calculated as $J_X = ([X]_p \times V_p - [X]_c \times V_c)/(L \times t)$, where $[X]_p$ and $[X]_c$ are the concentrations of ion X in the perfusate and collectate, respectively; V_p and V_c are the perfusion and collection rates, respectively; L is the tubule length; and t is the collection time. V_p was calculated as $V_p = V_c \times [\text{creat}]_c/[\text{creat}]_p$, where $[\text{creat}]_c$ and $[\text{creat}]_p$ are the concentrations of creatinine in the collectate and perfusate, respectively. For each tubule, ion fluxes were averaged over the 4 collection periods. Microperfusion results were analyzed using a one-way ANOVA analysis followed by Bonferroni's Multiple Comparison test (Prism software).

Metabolic studies. Mice were individually housed in metabolic cages (Techniplast, France) with free access to a standard laboratory diet (2.8 g of Na^+ /kg; Safe France). After three days of acclimatization, 24h urine was collected. The mice were then switched to a high sodium diet (3% NaCl solution as drinking water) and urine was collected during the next 24h. Urinary creatinine concentrations were determined using an automatic analyzer (Konelab 20i; Thermo, France) and urinary Na^+ concentration was determined by flame photometry (IL943, Instruments laboratory, France). Results were analyzed using a two-way ANOVA analysis followed by Bonferroni's Multiple Comparison test (Prism software).

Mathematical model description

The main Na^+, K^+, and Cl^- transport pathways in the mouse CCD are illustrated in Figure 1. In principal cells, the basolateral Na^+/K^+-ATPase generates the gradients needed to sustain Na^+ reabsorption via ENaC, as well as K^+ secretion via the renal outer medullary K^+ channel ROMK or K^+ recycling via basolateral K^+ channels. In type B intercalated cells, as proposed by Eladari and colleagues (Chambrey *et al.*, 2013), the net reabsorption of NaCl is energized by basolateral v-ATPase pumps. Na^+ enters the cell on the apical side via NDCBE and exits via AE4 on the basolateral side. The apical uptake of Cl^- is mediated by the Cl^-/HCO_3^- exchanger pendrin; a fraction of Cl^- is recycled via NDCBE while the remainder exits via the basolateral Cl^- channel ClC-K2. Note that this scheme assumes that AE4, the transport properties of which remain controversial, operates as a Na^+-HCO_3^-

cotransporter, with a Na^+:HCO_3^- stoichiometry of 1:3 as required for a sodium extruder (Boron, 2004). Type A intercalated cells express NKCC1 (Pech *et al.*, 2012), ClC-K2 (Kobayashi *et al.*, 2001; Nissant *et al.*, 2006), and the K^+-Cl^- cotransporter KCC4 (Boettger *et al.*, 2002) on the basolateral side. At the apical membrane, we assume the presence of K^+ and Cl^- channels, as suggested by Pech et al. (Pech *et al.*, 2012) and discussed below. We also assume that Na^+ can be extruded apically by H^+/K^+-ATPase type 2 (HKA2) pumps, as described below, since those pumps may extrude Na^+ instead of protons in exchange for K^+ (Grishin *et al.*, 1996; Cougnon *et al.*, 1998; Crambert *et al.*, 2002).

The mathematical model describes the transepithelial reabsorption or secretion of water and solutes along the full length of the CCD, via paracellular and transcellular pathways. It is conceptually similar to the rat CCD model developed by Weinstein (Weinstein, 2001), with significant differences in morphology and in the presence and/or activity of some transporters, as detailed below. We distinguish 6 compartments: the lumen (denoted by the superscript L), principal cells (P), type A (A) and B (B) intercalated cells, the extracellular (i.e., lateral) space between cells (E), and the peritubular solution (S). We account for the transport of the following solutes in addition to water: Na^+, K^+, Cl^-, HCO_3^-, H_2CO_3, CO_2, NH_3, NH_4^+, HPO_4^{2-}, $H_2PO_4^-$, and H^+. The composition of the luminal fluid is specified at the CCD entrance, and that of the peritubular space is fixed. At a given position along the tubule (taken to be 1 mm long), the volume, electric potential and solute concentrations in the lumen and cells are obtained by solving steady-state conservation equations for volume, charge, and mass, respectively. A summary of the steady-state conservation equations for volume, charge, and mass, can be found in references (Weinstein, 2001; Bonny & Edwards, 2013). The specific characteristics of this mouse CCD model are described below.

***Morphological parameters*.** The morphological parameters of the mouse CCD are determined under *ex vivo* conditions. Based upon our (unpublished) measurements, the outer diameter (D_o) is estimated as 51 μm, and the inner diameter (D_i) as 27.5 μm; note that the latter value is used to normalize by the epithelial surface area. The epithelial volume is thus computed as 16.8 $\mu m^3/\mu m^2$ epithelium (or 16.8×10^{-4} cm^3/cm^2 epithelium).

Excluding non-A non-B and bipolar cells, the fraction of P, A, and B cells in mouse CCD is taken as 71.5 %, 21.5%, and 7.0%, respectively (Kim *et al.*, 1999). In the absence of mouse data, we assume that the lateral space represents 10% of epithelial volume, as in rabbits (Welling *et al.*, 1981), and that individual cells occupy the same volume under basal conditions. With these hypotheses, the aggregate volume of P, A, and B cells is respectively computed as 10.8x10^{-4}, 3.2x10^{-4}, and 1.1x10^{-4} cm^3/cm^2 epithelium.

Membrane surface areas are determined assuming that the cuboidal cells are comprised between two co-axial cylinders of diameters D_i and D_o, there are roughly 4 cells per cross-section, all cells have the same (axial) height, and the area occupied by tight junctions represents 1% of the epithelial surface area, vs. 5% for the basement membrane. Examination of cell shape and surface areas in mouse CCDs (unpublished observations) suggests that membrane infolding increase basal membrane areas approximately 5-fold, and lateral membrane areas 2-fold, in all cell types. Infolding appears to enhance the apical membrane area more in intercalated cells (by a factor of ~ 4) than in principal cells (by a factor of ~ 2). Morphological parameter values are summarized in **Table 1**.

Permeability values. To match our experimental results, the water permeability per unit surface area (denoted P_f) of the principal cell apical membranes is set to 10 μm s^{-1} in the absence of ADH. The basolateral-to-apical membrane P_f ratio as is taken as 3.5 (Harris *et al.*, 1991) and the P_f of intercalated cell membranes is assumed to be 1,000 times lower than that of corresponding principal cell membranes. The water permeability of the tight junction is taken as 0.0040 cm^3 s^{-1} per cm^2 epithelial area, and that of the basement membrane as 1.80 cm^3 s^{-1} per cm^2 epithelial area, as in the rat model (Weinstein, 2001).

Solute permeability values are identical to those of the rat CCD model, except for the following modifications (recapitulated in **Table 2**). The background H^+ permeability of all cell membranes is set to zero. In principal cells, the apical membrane is taken to be impermeable to Cl^- and HCO_3^-, and the basolateral permeability to Cl^- is chosen as

0.002×10^{-5} cm s^{-1}. The permeability of ENaC and ROMK are respectively set to 0.67×10^{-5} and 2.50×10^{-5} cm s^{-1}.The apical membrane of A cells includes conductive pathways for K^+ (0.30×10^{-5} cm s^{-1}) and Cl^- (6.0×10^{-5} cm s^{-1}), but not to HCO_3^-; the A cell basolateral permeability to Cl^- is set to 0.50×10^{-5} cm s^{-1}, and that to K^+ to 0.125×10^{-5} cm s^{-1}. Note that the contribution of K^+ to the basolateral conductance in intercalated cells, thought to be small in rabbit CCD (Muto *et al.*, 1990), is more significant in rat CCD (Schlatter & Schafer, 1988). In B cells, the basolateral permeability to HCO_3^- is zero, and HCO_3^- exits the cell via AE4 instead. Note that, unless otherwise noted, the background permeability to HCO_3^- is taken as 20% of that to Cl^-, and the background permeability to NH_4^+ as 20% of that to K^+ (Weinstein, 2001). The permeabilities of the basement membrane, taken to be the same in mice and rats (per cm^2 epithelial area), yield a conductance of ~ 1000 mS cm^{-2}.

Membrane transporters. In contrast to the rat CCD model (Weinstein, 2001), the present model incorporates the recently identified transporters mediating Na^+ reabsorption across B cells, namely NDCBE and AE4. It also includes NKCC1, KCC4, as well as apical K^+ and Cl^- channels in A cells. Conversely, it assumes there are no apical NaCl co-transporters in principal cells and no basolateral Cl^-/HCO_3^- exchangers in B cells. Solute fluxes across ClC-K2, NHE1, pendrin, and Na^+/K^+-ATPase pumps are also formulated differently than in the rat model. Corresponding flux expressions are described in the **Appendix**. Main solute permeability values and transporter densities are respectively given in **Tables 2 and 3**.

RESULTS

We measured solute transport in isolated, microperfused CCDs of Na^+-depleted mice; a low-sodium diet has been shown to stimulate NaCl reabsorption, whereas the net transepithelial fluxes of Na^+ and Cl^- are insignificant under a normal diet (Leviel *et al.*, 2010). So as to mimic *in vivo* conditions, the CCDs were perfused with a hypo-osmotic solution (184 mOsm/kg H_2O) that contained less Na^+, Cl^-, and HCO_3^-, and more K^+ than the bath (Buerkert *et al.*, 1983; Elalouf *et al.*, 1984; Beck *et al.*, 1988), as specified above. The contribution of the different transcellular and paracellular pathways to net transepithelial fluxes was assessed by adding specific inhibitors to the perfusion solution or the bath.

Characterization of the paracellular pathway

To assess the contribution of the paracellular route to Na^+ and Cl^- transport in mouse CCDs, we first inhibited NaCl transport across transcellular routes: ENaC and the NDCBE-pendrin pathway were respectively blocked by infusing amiloride and hydrochlorothiazide (HCTZ) in the lumen, and transport pathways in type A intercalated cells were blocked by adding Schering 28080 (an inhibitor of H^+/K^+-ATPase types 1 and 2) to the perfusate and bumetanide in the bath. Under these conditions (referred to as the “paracellular” case), as shown in Figure 2A-D, the CCD secreted Na^+ (J_{Na} = - 16.8 ± 0.8 pmol/min/mm; n = 5) whereas the Cl^- flux was negligible (J_{Cl} = - 3.4 ± 2.4 pmol/min/mm); the transepithelial voltage (denoted ΔV_{te}) was – 12.8 ± 1.8 mV. By fitting the parameters of our mathematical model to these flux and voltage values, we estimated the permeabilities of the paracellular pathway to Na^+ and Cl^- as 0.35×10^{-5} and 0.42×10^{-5} cm s^{-1}, respectively. These values are consistent with the Cl^-:Na^+ permeability ratio of 1.2 measured in rat CCD (Schafer & Troutman, 1990). We should nevertheless recognize that there is some uncertainty in our Cl^- permeability estimate because the measured paracellular Cl^- flux is small, due to the counterbalancing effects of the transepithelial electric potential difference and the Cl^- concentration gradient, and experimental variations are thus large in relative terms. As shown in Figure 3, the model predicts that owing to these counteracting effects, the Cl^- flux across the tight junction changes direction along the CCD.

Under the same conditions, the CCD reabsorbed K^+ (J_K = 16.3 ± 2.5 pmol/min/mm, Fig 2C). The cocktail of inhibitors that we used does not necessarily abolish all transcellular K^+ transport because most cells display apical and basolateral K^+ channels. Assuming an intracellular concentration of K^+ of 140 mM, our model predicts that in the presence of 15 mM and 4 mM of potassium at the lumen entrance and in the bath respectively, the electrochemical gradient of K^+ across the apical membrane is favorable to its entry into the cell whereas that across the basolateral membrane is favorable to its exit (Figure 3). Our model predictions matched K^+ flux measurements well assuming that the K^+ permeability of the paracellular pathway is three times that of Na^+ (i.e., 1.05×10^{-5} cm s^{-1}), as previously reported in rats treated with desoxycorticosterone (29) .

The tight junctional conductance (G_{TJ}) of the mouse CCD was then computed as 3.3 mS cm^{-2}, which is similar to reported values for the rabbit CCD (Stoner *et al.*, 1974; Koeppen & Giebisch, 1985). Two other studies of mouse CCD reported larger transepithelial conductance values (G_T ~ 10 mS cm^{-2}), but they did not distinguish between paracellular and transcellular pathways (Lehrmann *et al.*, 2002; Pech *et al.*, 2007). In rats treated with DOCA, G_{TJ} was determined as 11 to 13 mS cm^{-2} ; note, however, that a model of the rat CCD had to assume a much lower conductance (i.e., 5 mS cm^{-2}) to avoid unrealistic backflux values (Weinstein, 2001).

Contribution of principal cells

To estimate transport rates across principal cells, we then measured ion fluxes in the presence of HCTZ, Schering 28080, and bumetanide, but in the absence of amiloride (conditions referred to as "paracellular + PC"). Under the same asymmetric conditions as above, removal of amiloride abolished sodium secretion (J_{Na} = -4.6 ± 2.2 pmol/min/mm - n = 5; $p < 0.05$; Fig 2A) but did not significantly alter chloride and potassium fluxes (J_{Cl} = -0.4 ± 1.4 pmol/min/mm; J_K = 14.2± 1.6 pmol/min/mm; Fig 2B-C), nor the electric potential difference (ΔV_{te} = -18.3 ± 4.7 mV; Fig 2D). In other words, Na^+ reabsorption across principal cells approximately counterbalanced Na^+ secretion via the paracellular route under asymmetric conditions.

Sodium secretion in the presence of amiloride

Conversely, we assessed the contribution of intercalated cells by measuring fluxes in the presence of amiloride only, under the same asymmetric conditions (the “paracellular + IC” case). Compared with the “paracellular” case, removing the inhibitors of transport pathways in type A and type B intercalated cells increased the secretion of Na^+ (J_{Na} = -32.7 ± 4.7 pmol/min/mm, n = 9, $p<0.01$, Fig 2A) as well as the reabsorption of K^+ (J_K = 22.1 ± 1.5 pmol/min/mm; $p<0.01$; Fig 2C), without altering significantly Cl^- fluxes (J_{Cl} = - 7.8 ± 3.8 pmol/min/mm) nor the transepithelial voltage (ΔV_{te} = -8.8 ± 2.2 mV). These results, summarized in **Table 4**, indicate that type A and/or type B intercalated cells mediate Na^+ secretion and K^+ reabsorption.

Sodium secretion in the presence of bumetanide and amiloride

According to our hypothesis (see ***Introduction***), type A intercalated cells could secrete Na^+ by mediating the basolateral entry of Na^+ and Cl^- along with K^+ via the NKCC1 cotransporter. To confirm the involvement of type A intercalated cells in Na^+ secretion, we evaluated the effect of adding bumetanide to the bath. In the presence of both amiloride and bumetanide, the secretion of Na^+ was significantly attenuated (J_{Na} = - 18.4 ± 1.8 pmol/min/mm; $p<0.05$; n = 5; Fig 4A) compared to that in the presence of amiloride only, and the secretion of Cl^- was abolished (J_{Cl} = 1.4 ± 1.8 pmol/min/mm) but was not significantly different from that measured in the presence of amiloride only (Fig 4B). The addition of bumetamide in the presence of amiloride did not affect K^+ reabsorption nor the transepithelial voltage (Fig 4C-D). These results strongly suggest that the secretion of Na^+ by intercalated cells originates from type A intercalated cells and is mediated by NKCC1 at the basolateral membrane.

As predicted by the model, the addition of bumetanide (in the presence of amiloride) has only a small impact on K^+ reabsorption across type A cells because of compensatory mechanisms. NKCC1 inhibition leads to a large reduction in intracellular Na^+ and Cl^-, which down-regulates the activity of apical HKA2 pumps, but this is partially offset by a large decrease in apical K^+ secretion via K^+ channels, as illustrated in Figure 5.

Role of H^+/K^+-ATPase type 2 in Na^+ secretion

We next investigated the apical pathways that might support Na^+ secretion in type A intercalated cells. The existence of Cl^- channels at the apical membrane was proposed by Pech et al. (Pech *et al.*, 2012), but the mechanisms by which Na^+ may be extruded apically remain unknown. Our calculations indicate that secondary active Na^+ exit is theoretically possible via apical Na^+-HCO_3^- cotransporters and/or NCBDE, both of which would couple the extrusion of Na^+ to that of HCO_3^-. Since the main role of type A cells is to acidify the lumen, a secretion scheme involving these transporters is unlikely. Another candidate is H^+/K^+-ATPase type 2 (HKA2), which can pump out Na^+ instead of protons in exchange for K^+ (Grishin *et al.*, 1996; Cougnon *et al.*, 1998; Crambert *et al.*, 2002), and which is expressed apically in type A cells in the rat CCD (Wingo *et al.*, 1990; Bastani, 1995).
To determine whether HKA2 mediates transcellular Na^+ secretion, we measured ion fluxes across the CCD of HKA2-null mice, under the same asymmetric conditions as above, in the presence of amiloride. As shown in Figure 4A, Na^+ secretion fluxes in HKA2-null mice were significantly attenuated compared to those in wild-type mice under identical conditions ($J_{Na} = -17.0 \pm 1.5$ pmol/min/mm; n = 6; p<0.01) and were similar to those measured in the presence of bumetanide in WT mouse CCDs. Cl^- and K^+ fluxes, as well as the transepithelial voltage, were not modified in HKA2-null mice (Fig 4B-D). These results demonstrate the involvement of $H^+(Na^+)/K^+$-ATPase type 2 in apical Na^+ exit in type A intercalated cells.

Sodium transport in the absence of inhibitors

We used the previous results to calibrate the mathematical model, specifically to estimate the density of the transcellular transporters of Na^+, K^+, and Cl^- (**Table 3**). We then predicted net transepithelial fluxes under asymmetric conditions in the absence of inhibitors (Figure 6). Assuming a perfusion rate of 2.0 nl/min and a fixed tubular length of

1 mm, the predicted fluxes of Na^+, Cl^-, and K^+ were respectively equal to -11.4, 3.1, and 12.3 pmol/min/mm. Subsequent measurements of these fluxes *in vitro* yielded good agreement between theoretical and experimental values (Figure 7): the measured fluxes of Na^+, Cl^-, and K^+ were respectively – 8.2 ± 1.6, -1.3 ± 1.3, and 12.0 ± 0.9 pmol/min/mm. Note that the model predicts that inhibiting apical proton secretion via H^+-ATPase has a negligible impact on J_{Na}, J_K, and J_{Cl} (results not shown).

Physiological relevance of the Na^+ secretion pathway

To assess the physiological relevance of HKA2-mediated Na^+ secretion in the collecting duct, we measured the renal response to Na^+ loading of WT and HKA2-null mice. There was no difference in the daily Na^+ intake of WT and HKA2-null mice under either a normal or a high salt diet (Fig 8A). However, whereas urinary Na^+ excretion was similar between both strains under normal conditions, one day after the switch from a normal to a high salt diet, HKA2-null mice excreted ~ 40% less Na^+ than WT mice did (Fig 8B).

DISCUSSION

In this study 1) we demonstrated that type A intercalated cells of the mouse CCD have the ability to avidly secrete Na^+, 2) we found that *ex vivo* (i.e. in the absence of acute regulatory factors) and in the presence of physiological transepithelial concentration gradients, the CCD of Na^+-depleted mice paradoxically secretes Na^+ and reabsorbs K^+, and 3) we developed a mathematical model of ion transport in the mouse CCD that integrates the NaCl transport capacity of type A intercalated cells; model predictions fit fairly well the measured values of ion fluxes under all the experimental conditions we tested. These results raise several questions regarding 1) the mechanism of NaCl secretion in type A intercalated cells and its physiological regulation, 2) the differences in ion fluxes observed *ex vivo* between symmetrical and asymmetrical conditions, and 3) the discrepancy between the ion fluxes measured *ex vivo* and those expected to prevail *in vivo* in CCDs from Na^+-depleted mice, i.e. NaCl reabsorption in absence of net K^+ transport. These inter-related questions are addressed below by combining our experimental findings with data from the literature and the predictions of our mathematical model.

Mechanisms and regulation of NaCl secretion by type A intercalated cells

NaCl secretion across the CCD has been already observed under symmetric conditions such as in the presence of amiloride and thiazide (Leviel *et al.*, 2010), or in slc4a8- or slc4a9-knock-out mice (Chambrey *et al.*, 2013); since ΔV_{te} is lumen-positive in the presence of amiloride and thiazide, the secretion of Na^+ cannot occur across the paracellular route. Bumetanide-sensitive Na^+ secretion has also been reported in the rat outer medullary collecting duct (Wall & Fischer, 2002) and inner medullary collecting duct (Rocha & Kudo, 1990a). In the rabbit CCD, however, bumetanide does not affect net Na^+ reabsorption under symmetric conditions (Liu *et al.*, 2011).

Our flux measurements in WT and $HKA2^{-/-}$ mice strongly suggest that HKA2 mediates apical Na^+ exit from type A intercalated cells. HKA2 has been localized to the apical membrane of type A intercalated cells in the CCD and shown to be a versatile transporter regarding its cation specificity (for review see reference (Crambert, 2014)). Several experimental studies have demonstrated that HKA2 can extrude Na^+ instead of H^+ (Grishin *et al.*, 1996; Cougnon *et al.*, 1998; Crambert *et al.*, 2002), and a recent mathematical model of the pump suggests that it mediates mainly Na^+/K^+ exchange under physiological conditions (Nadal-Quiros *et al.*, 2015).

The physiological pertinence of Na^+ secretion across H^+/K^+-ATPase type 2 pumps was demonstrated here by our finding that HKA2$^{-/-}$ mice displayed an impaired ability to excrete a sodium load. In other words, HKA2 pumps play a significant role in excreting excess Na^+ following sodium loading.

The secretion of chloride across type A intercalated cells in mouse CCD was demonstrated earlier by Wall and colleagues (Pech *et al.*, 2012). In the present study, there was a similar tendency for Cl^- secretion across type A cells but it did not reach statistical significance. The apical pathways mediating the secretion of Cl^- in type A cells remain to be characterized. The contribution of Cl^- to the apical membrane resistance in intercalated cells appears to be small, at least in rat CCD (Schlatter & Schafer, 1988). However, the study of Pech et al. indicates that the apical Cl^- flux across type A cells is modulated by the transepithelial voltage (Pech *et al.*, 2012), suggesting that it is mediated by an electrogenic transporter. One candidate is Slc26a11, an anion transporter that co-localizes with the vacuolar H^+-ATPase in the mouse CCD (in particular at the apical membrane of type A cells) and regulates its activity (Xu *et al.*, 2011). Slc26a11 was shown to operate both as a Cl^- channel and as a Cl^-/HCO_3^- exchanger in heterologous expression systems (Xu *et al.*, 2011). Its functional role *in vivo* has not been examined. Another, less likely, candidate is the cystic fibrosis transmembrane conductance regulator (CFTR), which forms apical Cl^- channels in cultures of principal cells from the mouse collecting duct (Lu *et al.*, 2010). Whether it is also expressed by intercalated cells remains unclear. Moreover, Pech et al. (Pech *et al.*, 2012) found that CFTR inhibition did not affect benzamil-sensitive Cl^- fluxes in microperfused CCDs. As illustrated in Figure 6, our model confirms that a two-step mechanism of NaCl secretion in type A cells involving basolateral

NaCl entry via NKCC1 and Na^+ and Cl^- apical exit via HKA2 and chloride channels, respectively, is thermodynamically feasible. According to this model, type A cells also reabsorb K^+ under asymmetrical conditions. Alternatively, apical Cl^- secretion in type A cells could be mediated by a cotransporter such as KCC; a chloride-dependent potassium flux has been described in rabbit CCD (Wingo, 1989). Model predictions were very similar when we replaced the apical K^+ and Cl^- channels with an apical KCC cotransporter (results not shown).

The existence of a NaCl secreting pathway in the CCD suggests that this nephron segment might be a target of natriuretic hormones such as atrial natriuretic factor (ANF) and guanylin peptides (Sindic & Schlatter, 2007) and of their common second messenger cyclic GMP. Classically, ANF is thought to exert natriuretic effects through inhibition of ENaC and nucleotide-gated channels in the inner medullary collecting duct (IMCD) (Theilig & Wu, 2015). However, the ANF receptor guanylyl cyclase A has been found in the intercalated cells of rat CCDs (Hirsch *et al.*, 2001), and in microperfused rat IMCDs, ANF not only reduces sodium reabsorption but also increases the furosemide-sensitive secretion of NaCl by the Na-K-Cl cotransport system (Rocha & Kudo, 1990b). Thus, ANF might also be natriuretic by stimulating NaCl secretion through type A intercalated cells in the CCD. This conclusion is consistent with the only available studies in CCDs which show that ANF reduces net sodium transport (Nonoguchi *et al.*, 1989) but has no effect on the lumen-to-bath Na^+ flux (Rouch *et al.*, 1991; Schlatter *et al.*, 1996).

Differences in ion fluxes between symmetrical and asymmetrical conditions

When CCDs from Na^+-depleted mice are microperfused under symmetric conditions, $J_{Na,}$ J_{Cl} and J_K are, respectively, on the order of 35, 15 and -5 pmol/min/mm in the absence of inhibitors (Leviel *et al.*, 2010). All else being equal, our mathematical model predicts that under symmetric conditions these fluxes would be approximately 24, 3 and -6 pmol/min/mm respectively (**Table 5**). This indicates that abolishing the ion concentration gradients and/or hypo-osmolality of the apical fluid augments substantially the net reabsorption of chloride and sodium.

Data from the literature show that the paracellular permeability of the tight junction to Na^+ and Cl^- is decreased two-fold in symmetric conditions as compared to apical hypotonic conditions (Tokuda *et al.*, 2008), likely in response to inhibition of with-no-lysine kinase 4 (WNK) (Kahle *et al.*, 2004). Our mathematical model predicts that this increases only slightly the net fluxes of Na^+ and Cl^- (**Table 5**).

Intuitively, one would expect that increasing Cl^- reabsorption can be achieved either by stimulating ENaC (via its effect on the transepithelial voltage), by stimulating pendrin, or by inhibiting NaCl secretion by type A intercalated cells. The model predicts that a slight increase in ENaC activity increases Cl^- reabsorption through the paracellular pathway via its effect on ΔV_{te} but simultaneously increases Na^+ reabsorption and K^+ secretion. Inhibition of transporter activity in type A cells (NKCC1, HKA2 and apical Cl^- channels) hardly increases Cl^- reabsorption up to the observed level and markedly increases Na^+ reabsorption. It is only when we simulate an increase in pendrin activity that all predicted values (Na^+, K^+, and Cl^- fluxes and ΔV_{te}) are close to measured values under symmetric conditions (**Table 5**). This suggests that pendrin activity might be higher under symmetric relative to asymmetric conditions.

The mechanism by which pendrin activity might be inhibited under asymmetric conditions remains unknown. In asymmetric conditions, the concentration of Cl^- in the cytosol of type B intercalated cells is predicted to be significantly higher than under symmetric conditions (27.7 vs. 15.7 mM at the tubule mid-point). This might inactivate with-no-lysine kinase 3 which has been described as a putative chloride-sensing kinase (Pacheco-Alvarez & Gamba, 2011), and in turn modulate the activity of pendrin.

Discrepancy between the ion fluxes measured ex vivo and those expected to prevail in vivo in CCDs from Na^+-depleted mice

The most puzzling finding of this study is that the CCD of Na^+-depleted mice, when perfused with a hypo-osmotic solution the composition of which mimics *in vivo* conditions, secretes Na^+ and reabsorbs K^+. In that sodium-deprived state, we expected the CCD to mediate net NaCl reabsorption and no K^+ transport so as to maintain sodium homeostasis and blood pressure without affecting the potassium balance. It is likely that the discrepancy between *ex vivo* and *in vivo* conditions stems from the absence in the former condition of regulatory factors modulating one or several transport pathways.

The most likely candidate is angiotensin 2, the concentration of which is increased in Na^+-depleted states. Angiotensin 2 is known to stimulate pendrin (Pech *et al.*, 2007) and ENaC (Zaika *et al.*, 2013) without altering ROMK activity (Wei *et al.*, 2014). Our model predicts that doubling the activity of ENaC and pendrin induces significant NaCl reabsorption without K^+ secretion under asymmetric conditions (J_{Na} = 15.5, J_{Cl} = 20.1, J_K = -0.2 pmol/min/mm).

In conclusion, we found that type A intercalated cells in the mouse cortical collecting duct have the capacity to significantly secrete Na^+: this secretion is mediated, at least in part, by H^+/K^+-ATPase type 2 pumps on the apical side and by a bumetanide-sensitive pathway on the basolateral side. These results demonstrate for the first time that, contrary to the classical view, the CCD mediates Na^+ secretion in the presence of physiological concentration gradients, and that its ability to reabsorb NaCl *in vivo* is regulated in an acute manner by hormonal and neural factors. The capacity of the CCD to simultaneously activate reabsorption routes and inhibit secretion pathways, or vice-versa, should allow this segment to adapt to a wide range of conditions at a small energetic cost.

REFERENCES

Azroyan A, Laghmani K, Mordasini D, Doucet A & Edwards A. (2011). Regulation of pendrin by pH: dependence on glycosylation. *Biochem J* **434,** 61-72.

Bastani B. (1995). Colocalization of H-ATPase and H,K-ATPase immunoreactivity in the rat kidney. *Journal of the American Society of Nephrology* **5,** 1476-1482.

Beck FX, Dorge A, Rick R, Schramm M & Thurau K. (1988). The distribution of potassium, sodium and chloride across the apical membrane of renal tubular cells: effect of acute metabolic alkalosis. *Pflugers Archiv* **411,** 259-267.

Biemesderfer D, Reilly RF, Exner M, Igarashi P & Aronson PS. (1992). Immunocytochemical characterization of Na(+)-H+ exchanger isoform NHE-1 in rabbit kidney. *American Journal of Physiology - Renal Physiology* **263,** F833-F840.

Boettger T, Hubner CA, Maier H, Rust MB, Beck FX & Jentsch TJ. (2002). Deafness and renal tubular acidosis in mice lacking the K-Cl co-transporter Kcc4. *Nature* **416,** 874-878.

Bonny O & Edwards A. (2013). Calcium reabsorption in the distal tubule: regulation by sodium, pH, and flow. *American Journal of Physiology - Renal Physiology* **304,** F585-F600.

Boron WF. (2004). Regulation of intracellular pH. *Advan Physiol Edu* **28,** 160-179.

Buerkert J, Martin D & Trigg D. (1983). Segmental analysis of the renal tubule in buffer production and net acid formation. *American Journal of Physiology - Renal Physiology* **244,** F442-F454.

Chambrey R, Kurth I, Peti-Peterdi J, Houillier P, Purkerson JM, Leviel F, Hentschke M, Zdebik AA, Schwartz GJ, Hubner CA & Eladari D. (2013). Renal intercalated cells are rather energized by a proton than a sodium pump. *Proceedings of the National Academy of Sciences* **110,** 7928-7933.

Cougnon M, Bouyer P, Planelles G & Jaisser F. (1998). Does the colonic H,K-ATPase also act as an Na,K-ATPase? *Proceedings of the National Academy of Sciences* **95,** 6516-6520.

Crambert G. (2014). H-K-ATPase type 2: relevance for renal physiology and beyond. *American Journal of Physiology - Renal Physiology* **306,** F693-F700.

Crambert G, Horisberger J-D, Modyanov NN & Geering K. (2002). Human nongastric H+-K+-ATPase: transport properties of ATP1al1 assembled with different beta -subunits. *Am J Physiol Cell Physiol* **283,** C305-314.

Elalouf JM, Roinel N & Rouffignac C. (1984). Effects of antidiuretic hormone on electrolyte reabsorption and secretion in distal tubules of rat kidney. *Pflügers Archiv European Journal of Physiology* **401,** 167-173.

Fuster D, Moe OW & Higelmann DW. (2008). Steady-state function of the ubiquitous mammalian Na/H exchanger (NHE1) in relation to dimer coupling models with 2Na/2H stoichiometry. *J Gen Physiol* **132,** 465-480.

Grishin AV, Bevensee MO, Modyanov NN, Rajendran V, Boron WF & Caplan MJ. (1996). Functional expression of the cDNA encoded by the human ATP1AL1 gene. *American Journal of Physiology - Renal Physiology* **271,** F539-F551.

Harris HW, Strange K & Zeidel ML. (1991). Current understanding of the cellular biology and molecular structure of the anti-diuretic hormone-stimulated water transport pathway. *J Clin Invest* **88,** 1-8.

Hirsch JR, Kruhoffer M, Adermann K, Heitland A, Maronde E, Meyer M, Forssmann W-G, Herter P, Plenz G & Schlatter E. (2001). Cellular localization, membrane distribution, and possible function of guanylyl cyclases A and 1 in collecting ducts of rat. *Cardiovascular Research* **51,** 553-561.

Kahle KT, MacGregor GG, Wilson FH, Van Hoek AN, Brown D, Ardito T, Kashgarian M, Giebisch G, Hebert SC, Boulpaep EL & Lifton RP. (2004). Paracellular Cl- permeability is regulated by WNK4 kinase: Insight into normal physiology and hypertension. *Proceedings of the National Academy of Sciences* **101,** 14877-14882.

Kim JIN, Kim Y-H, Cha J-H, Tisher CC & Madsen KM. (1999). Intercalated cell subtypes in connecting tubule and cortical collecting duct of rat and mouse. *Journal of the American Society of Nephrology* **10,** 1-12.

Kobayashi K, Uchida S, Mizutani S, Sasaki SEI & Marumo F. (2001). Intrarenal and cellular localization of CLC-K2 protein in the mouse kidney. *Journal of the American Society of Nephrology* **12,** 1327-1334.

Koeppen B & Giebisch G. (1985). Cellular electrophysiology of potassium transport in the mammalian cortical collecting tubule. *Pflugers Archiv* **405,** S143-S146.

Lehrmann H, Thomas J, Kim SJ, Jacobi C & Leipziger J. (2002). Luminal P2Y2 receptor-mediated inhibition of Na+ absorption in isolated perfused mouse CCD. *Journal of the American Society of Nephrology* **13,** 10-18.

Leviel F, Hubner CA, Houillier P, Morla L, El Moghrabi S, Brideau G, Hatim H, Parker MD, Kurth I, Kougioumtzes A, Sinning A, Pech V, Riemondy KA, Miller RL, Hummler E, Shull GE, Aronson PS, Doucet A, Wall SM, Chambrey Rg & Eladari D. (2010). The Na+-dependent chloride-bicarbonate exchanger SLC4A8 mediates an electroneutral Na+ reabsorption process in the renal cortical collecting ducts of mice. *The Journal of Clinical Investigation* **120,** 1627-1635.

Liu W, Schreck C, Coleman RA, Wade JB, Hernandez Y, Zavilowitz B, Warth R, Kleyman TR & Satlin LM. (2011). Role of NKCC in BK channel-mediated net K+ secretion in the CCD. *American Journal of Physiology - Renal Physiology* **301,** F1088-F1097.

Lourdel S, Paulais M, Marvao P, Nissant A & Teulon J. (2003). A chloride channel at the basolateral membrane of the distal convoluted tubule: a candidate ClC-K channel. *J Gen Physiol* **121,** 287-300.

Lu M, Dong K, Egan ME, Giebisch GH, Boulpaep EL & Hebert SC. (2010). Mouse cystic fibrosis transmembrane conductance regulator forms cAMP-PKA-regulated apical chloride channels in cortical collecting duct. *Proceedings of the National Academy of Sciences* **107,** 6082-6087.

Meneton P, Schultheis PJ, Greeb J, Nieman ML, Liu LH, Clarke LL, Duffy JJ, Doetschman T, Lorenz JN & Shull GE. (1998). Increased sensitivity to K+ deprivation in colonic H,K-ATPase-deficient mice. *The Journal of Clinical Investigation* **101,** 536-542.

Muto S, Yasoshima K, Yoshitomi K, Imai M & Asano Y. (1990). Electrophysiological identification of alpha- and beta-intercalated cells and their distribution along the rabbit distal nephron segments. *The Journal of Clinical Investigation* **86,** 1829-1839.

Nadal-Quiros M, Moore LC & Marcano M. (2015). Parameter estimation for mathematical models of a nongastric H+(Na+)-K+(NH4+)-ATPase. *American Journal of Physiology - Renal Physiology* **309,** F434-F446.

Nissant A, Paulais M, Lachheb S, Lourdel S & Teulon J. (2006). Similar chloride channels in the connecting tubule and cortical collecting duct of the mouse kidney. *American Journal of Physiology - Renal Physiology* **290,** F1421-F1429.

Nonoguchi H, Sands JM & Knepper MA. (1989). ANF inhibits NaCl and fluid absorption in cortical collecting duct of rat kidney. *American Journal of Physiology - Renal Physiology* **256,** F179-F186.

Pacheco-Alvarez D & Gamba G. (2011). WNK3 is a putative chloride-sensing kinase. *Cellular Physiology and Biochemistry* **28,** 1123-1134.

Pech V, Thumova M, Kim YH, Agazatian D, Hummler E, Rossier BC, Weinstein AM, Nanami M & Wall SM. (2012). ENaC inhibition stimulates Cl- secretion in the mouse cortical collecting duct through an NKCC1-dependent mechanism. *American Journal of Physiology - Renal Physiology* **303,** F45-F55.

Pech Vr, Kim YH, Weinstein AM, Everett LA, Pham TD & Wall SM. (2007). Angiotensin II increases chloride absorption in the cortical collecting duct in mice through a pendrin-dependent mechanism. *American Journal of Physiology - Renal Physiology* **292,** F914-F920.

Rocha AS & Kudo LcH. (1990a). Factors governing sodium and chloride transport across the inner medullary collecting duct. *Kidney International* **38,** 654-667.

Rocha AS & Kudo LH. (1990b). Atrial peptide and cGMP effects on NaCl transport in inner medullary collecting duct. *Am J Physiol Renal Physiol* **259,** F258-268.

Rouch AJ, Chen L, Troutman SL & Schafer JA. (1991). Na+ transport in isolated rat CCD: effects of bradykinin, ANP, clonidine, and hydrochlorothiazide. *American Journal of Physiology - Renal Physiology* **260,** F86-F95.

Schafer JA & Troutman SL. (1990). cAMP mediates the increase in apical membrane Na+ conductance produced in rat CCD by vasopressin. *American Journal of Physiology - Renal Physiology* **259,** F823-F831.

Schlatter E, Cermak R, Forssmann WG, Hirsch JR, Kleta R, Kuhn M, Sun D & Schafer JA. (1996). cGMP-activating peptides do not regulate electrogenic electrolyte transport in principal cells of rat CCD. *American Journal of Physiology - Renal Physiology* **271,** F1158-F1165.

Schlatter E & Schafer JA. (1988). Electrophysiological studies in intercalated cells of rat cortical collecting tubules. *Pflugers Archiv* **411,** Suppl 1 R101.

Sindic A & Schlatter E. (2007). Renal electrolyte effects of guanylin and uroguanylin. *Curr Opin Nephrol Hypertens* **16,** 10-15.

Stoner LC, Burg MB & Orloff J. (1974). Ion transport in cortical collecting tubule; effect of amiloride. *American Journal of Physiology -- Legacy Content* **227,** 453-459.

Strieter J, Stephenson JL, Giebisch G & Weinstein AM. (1992). A mathematical model of the rabbit cortical collecting duct. *Am J Physiol Renal Physiol* **263,** F1063-F1075.

Summa V, Camargo SMR, Bauch C, Zecevic M & Verrey F. (2004). Isoform specificity of human Na+,K+-ATPase localization and aldosterone regulation in mouse kidney cells. *The Journal of Physiology* **555,** 355-364.

Terada Y & Knepper MA. (1990). Thiazide-sensitive NaCl absorption in rat cortical collecting duct. *Am J Physiol Renal Physiol* **259,** F519-528.

Theilig F & Wu Q. (2015). ANP-induced signaling cascade and its implications in renal pathophysiology. *Am J Physiol Renal Physiol* **308,** F1047-1055.

Tokuda S, Niisato N, Nakajima K & Marunaka Y. (2008). Regulation of the paracellular Na+ and Cl- conductances by the NaCl-generated osmotic gradient in a manner dependent on the direction of osmotic gradients. *Biochem Biophys Res Commun* **366,** 464-470.

Wall SM & Fischer MP. (2002). Contribution of the Na+-K+-2Cl- cotransporter (NKCC1) to transepithelial transport of H+, NH4+, K+, and Na+ in rat outer medullary collecting duct. *Journal of the American Society of Nephrology* **13,** 827-835.

Wall SM, Kim YH, Stanley L, Glapion DM, Everett LA, Green ED & Verlander JW. (2004). NaCl Restriction Upregulates Renal Slc26a4 Through Subcellular Redistribution: Role in Cl- Conservation. *Hypertension* **44,** 982-987.

Wei Y, Liao Y, Zavilowitz B, Ren J, Liu W, Chan P, Rohatgi R, Estilo G, Jackson EK, Wang WH & Satlin LM. (2014). Angiotensin II type 2 receptor regulates ROMK-like K(+) channel activity in the renal cortical collecting duct during high dietary K(+) adaptation. *Am J Physiol Renal Physiol* **307,** F833-843.

Weinstein AM. (1992). Chloride transport in a mathematical model of the rat proximal tubule. *American Journal of Physiology - Renal Physiology* **263,** F784-F798.

Weinstein AM. (2001). A mathematical model of rat cortical collecting duct: determinants of the transtubular potassium gradient. *American Journal of Physiology - Renal Physiology* **280,** F1072-F1092.

Weinstein AM. (2010). A mathematical model of rat ascending Henle limb. I. Cotransporter function. *American Journal of Physiology - Renal Physiology* **298,** F512-F524.

Welling LW, Evan AP & Welling DJ. (1981). Shape of cells and extracellular channels in rabbit cortical collecting ducts. *Kidney Int* **20,** 211-222.

Wingo CS. (1989). Reversible chloride-dependent potassium flux across the rabbit cortical collecting tubule. *American Journal of Physiology - Renal Physiology* **256,** F697-F704.

Wingo CS, Madsen KM, Smolka A & Tisher CC. (1990). H-K-ATPase immunoreactivity in cortical and outer medullary collecting duct. *Kidney Int* **38,** 985-990.

Xu J, Barone S, Li H, Holiday S, Zahedi K & Soleimani M. (2011). Slc26a11, a chloride transporter, localizes with the vacuolar H+-ATPase of A-intercalated cells of the kidney. *Kidney Int* **80,** 926-937.

Zaika O, Mamenko M, Staruschenko A & Pochynyuk O. (2013). Direct activation of ENaC by angiotensin II: recent advances and new insights. *Curr Hypertens Rep* **15,** 17-24.

ADDITIONAL INFORMATION

COMPETING INTERESTS

None of the authors has any conflict of interest.

AUTHOR CONTRIBUTIONS

Conception and design of experiments: LM, AD, GC, AE

Collection, assembly, analysis, and interpretation of data: LM, CL, AD, GC, AE

Drafting and/or critically revising the article: AD, GC, AE

All authors have approved the final version of the manuscript and agree to be accountable for all aspects of the work. All persons designated as authors qualify for authorship, and all those who qualify for authorship are listed.

FUNDING

No funding was received for this study.

APPENDIX

Transepithelial fluxes

General expressions for water and solute fluxes are given in references (Weinstein, 2001; Bonny & Edwards, 2013). Described below are the fluxes that differ from the rat CCD model (Weinstein, 2001). Note that Ψ^M is the electric potential in compartment M, C_i^M is the concentration of a given solute i in M, and J_i^{MN} is flux of i from compartment M to compartment N.

***Coupled transport*.** Since the kinetic behavior of NDCBE, AE4 and NKCC1 has not been characterized experimentally, we use the non-equilibrium thermodynamics (NET) approach to determine solute fluxes across these transporters. The driving force is given by the net difference in electrochemical potentials across the membrane, and the flux of solute i is computed as:

$$J_i^{MN} = \sum_j L_{i,j}^{MN} (\overline{\mu}_j^M - \overline{\mu}_j^N) \tag{1}$$

where $L_{i,j}^{MN}$ is a matrix of coefficients that depend on the stoichiometry and expression of the transporter, and $\overline{\mu}_i^M$ is the electrochemical potential of solute i in compartment M:

$$\overline{\mu}_i^M = RT \ln C_i^M + z_i F \Psi^M \tag{2}$$

The NET formulation was previously used to describe transport across NDCBE in the basolateral membrane of the proximal tubule (Weinstein, 1992). In the CCD, NDCBE fluxes from the lumen to type B cells are determined as:

$$\begin{aligned} J_{Na}^{LB-NDCBE} &= L_{NDCBE}^{LB} \left[(\overline{\mu}_{Na}^L - \overline{\mu}_{Na}^B) + 2(\overline{\mu}_{HCO3}^L - \overline{\mu}_{HCO3}^B) - (\overline{\mu}_{Cl}^L - \overline{\mu}_{Cl}^B) \right] \\ &= L_{NDCBE}^{LB}\, RT \ln\left(\frac{C_{Na}^L (C_{HCO3}^L)^2 C_{Cl}^B}{C_{Na}^B (C_{HCO3}^B)^2 C_{Cl}^L} \right) \end{aligned} \tag{3}$$

$$J_{HCO3}^{LB-NDCBE} = 2 J_{Na}^{LB-NDCBE}, \qquad J_{Cl}^{LB-NDCBE} = -J_{Na}^{LB-NDCBE} \tag{4}$$

Similarly, the Na^+ and HCO_3^- fluxes across AE4, from type B cells to the peritubular solution, are calculated as:

$$\begin{aligned} J_{Na}^{BS-AE4} &= L_{AE4}^{BS}\left[(\bar{\mu}_{Na}^{B} - \bar{\mu}_{Na}^{S}) + 3(\bar{\mu}_{HCO3}^{B} - \bar{\mu}_{HCO3}^{S})\right] \\ &= L_{AE4}^{BS}\left[RT\ln\left(\frac{C_{Na}^{B}(C_{HCO3}^{B})^3}{C_{Na}^{S}(C_{CO3}^{S})^3}\right) - 2F(\psi^{B} - \psi^{S})\right] \end{aligned} \qquad (5)$$

$$J_{HCO3}^{BS-AE4} = 3J_{Na}^{BS-AE4} \qquad (6)$$

AE4 fluxes across from type B cells to lateral spaces are obtained by replacing “S” with “E” in Eqs. (5-6).

Using the same approach, NKCC1 fluxes from type A cells to the peritubular solution are given by:

$$J_{Na}^{AS-NKCC1} = L_{NKCC1}^{AS}\, RT\ln\left(\frac{C_{Na}^{A}C_{K}^{A}(C_{Cl}^{A})^2}{C_{Na}^{S}C_{K}^{S}(C_{Cl}^{S})^2}\right) \qquad (7)$$

$$J_{K}^{AS-NKCC1} = J_{Na}^{AS-NKCC1}, \qquad J_{Cl}^{AS-NKCC1} = 2J_{Na}^{AS-NKCC1} \qquad (8)$$

KCC4. Fluxes across the K^+-Cl^- cotransporter KCC4 are determined using the kinetic model of Weinstein (Weinstein, 2010). The reaction scheme assumes that K^+ binds to, and unbinds from, the carrier before Cl^-, and it accounts for the competitive replacement of K^+ by NH_4^+.

Pendrin. Corresponding fluxes are computed based upon our kinetic model of Cl^-/HCO_3^- and Cl^-/OH^- exchange across pendrin (Azroyan *et al.*, 2011; Bonny & Edwards, 2013).

Basolateral Na^+/K^+-ATPase. The Na^+ and K^+ fluxes across Na^+/K^+-ATPase pumps between cell M (M = P, A, B) and the peritubular solution S are calculated as:

$$J_{Na}^{MS-NaK} = J_{\max}^{MS-NaK}\left[\frac{C_{Na}^{M}}{C_{Na}^{M} + K_{m,Na}^{NaK}}\right]^3\left[\frac{C_{K}^{S}}{C_{K}^{S} + K_{m,K}^{NaK}}\right]^2 \qquad (9)$$

$$J_{K}^{MS-NaK} = -(2/3)J_{Na}^{MS-NaK} \tag{10}$$

The affinity of the pump for sodium ($K_{m,Na}^{NaK}$) is fixed at 16.3 mM (Summa *et al.*, 2004), whereas that for potassium increases with the peritubular concentration of Na^+ (Strieter *et al.*, 1992):

$$K_{m,K}^{NaK} = 0.1\,(1 + C_{Na}^{S}/18.50) \tag{11}$$

Luminal H⁺(Na⁺)/K⁺(NH₄⁺)-ATPase. The non-gastric (or colonic, type 2) H^+/K^+-ATPase has been shown to mediate the exchange of Na^+ and K^+. As observed in vitro and in vivo, there is competitive binding between Na^+ and H^+ on the cytosolic side, and between K^+ and NH_4^+ on the luminal side. The fluxes of K^+, H^+, Na^+ and NH_4^+ across H^+/K^+-ATPase type 2 are determined using the recent kinetic model of the pump developed by Marcano and colleagues, assuming a $2H^+$:$2K^+$-per ATP stoichiometry (Nadal-Quiros *et al.*, 2015).

CLC-K2. The permeability of ClC-K2 in intercalated cells is taken to decrease with intracellular acidification (Lourdel *et al.*, 2003) and determined as:

$$h_{Cl}^{ClCK2} = h_{Cl}^{ClCK*}\exp[2.1\,(pH^{M} - 7.40)] \qquad 6.8 \le pH^{M} \le 8.0 \qquad \text{M = A, B} \tag{12}$$

where h_{Cl}^{ClCK*} is the ClC-K2 permeability to Cl^- at pHi = 7.40, respectively taken as $0.50\text{x}10^{-5}$ and $0.40\text{x}10^{-5}$ cm s^{-1} in type A and B cells.

NHE1. The basolateral membrane of principal cells expresses the Na^+/H^+ exchanger isoform NHE1 (Biemesderfer *et al.*, 1992). NHE1 fluxes are calculated using the parallel coupling model of Fuster et al. (Fuster *et al.*, 2008).

Table 1

Morphometric parameters of the mouse CCD

	Principal cells	Type A cells	Type B cells	Lateral interspace
Volume ($x10^{-4}$ cm^3/cm^2 epith)	10.79	3.25	1.06	1.68
Apical membrane area (cm^2/cm^2 epith)	1.42	0.85	0.277	0.01
Lateral membrane area (cm^2/cm^2 epith)	10.04	1.36	0.443	
Basal membrane area (cm^2/cm^2 epith)	6.56	1.97	0.643	0.05

The reference epithelial surface area is based upon the inner diameter of the lumen.

Table 2

Solute permeabilities of the mouse CCD

	Principal cells ($x10^{-5}$ cm.s^{-1})		Type A cells ($x10^{-5}$ cm.s^{-1})		Type B cells ($x10^{-5}$ cm.s^{-1})		Paracellular pathway ($x10^{-5}$ cm.s^{-1})
	apical	basolat	apical	basolat	apical	basolat	
Na^+	0.67	0	0	0	0	0	0.35
K^+	2.50	0.60	0.3	0.125	0	0.015	1.05
Cl^-	0	0.002	6	0.50	0	0.40	0.42
HCO_3^-	0	0.0004	0	0.10	0	0	0.084

"Apical" and "basolat" denote the apical and basolateral membranes of each cell type.

Basolateral chloride permeability values correspond to pHi = 7.40 (see Equation 12).

Table 3

Mouse CCD transporter density or maximum rate

	Principal cell	Type A cell	Type B cell
Na^+/K^+-ATPase	510×10^{-9} mmol s^{-1} cm^{-2} (basolateral)	75×10^{-9} mmol s^{-1} cm^{-2} (basolateral)	75×10^{-9} mmol s^{-1} cm^{-2} (basolateral)
H^+-ATPase		100×10^{-9} mmol cm^{-2} (apical)	$5{,}000 \times 10^{-9}$ mmol cm^{-2} (basolateral)
H^+/K^+-ATPase		3×10^{-9} mmol cm^{-2} (gastric,apical) 70×10^{-9} mmol cm^{-2} (non-gastric,apical)	6×10^{-9} mmol cm^{-2} (gastric,apical)
Basolateral Na^+/H^+ exchangers	0.2×10^{-9} mmol cm^{-2} (NHE1)	6×10^{-9} $mmol^2$ J^{-1} s^{-1} cm^{-2}	0.6×10^{-9} $mmol^2$ J^{-1} s^{-1} cm^{-2}
Basolateral Na_2HPO_4 cotransporters	0.20×10^{-9} $mmol^2$ J^{-1} s^{-1} cm^{-2}	0.08×10^{-9} $mmol^2$ J^{-1} s^{-1} cm^{-2}	0.08×10^{-9} $mmol^2$ J^{-1} s^{-1} cm^{-2}
Cl^-/HCO_3^- exchangers	0.2×10^{-9} $mmol^2$ J^{-1} s^{-1} cm^{-2} (basolateral)	20×10^{-9} mmol cm^{-2} (AE1, basolateral)	0.100×10^{-9} mmol cm^{-2} (pendrin, apical)
KCl cotransporters		0.06×10^{-9} mmol cm^{-2} (KCC4, basolateral)	
$Na(HCO_3^-)_3$ cotransporters			2500×10^{-9} $mmol^2$ J^{-1} s^{-1} cm^{-2} (AE4, basolateral)
Other NaCl transport pathways		60×10^{-9} $mmol^2$ J^{-1} s^{-1} cm^{-2} (NKCC1, basolateral)	400×10^{-9} $mmol^2$ J^{-1} s^{-1} cm^{-2} (NDCBE, apical)

Cortical collecting duct Na^+, K^+, and Cl^- transporter expression was chosen so that model predictions approximately match ionic fluxes measured under asymmetric conditions.

Table 4

Measured and calculated fluxes in the mouse CCD under asymmetric conditions

		J_{Na}	J_{Cl}	J_K	ΔV_{te}
WT, All inhibitors	Microperfusion (n = 5)	-16.8 ± 0.8 [-19.2; -14.4]	-3.4 ± 2.4 [-10.1; 3.4]	16.3 ± 2.5 [9.5; 23.1]	-12.8 ± 1.8 [-17.8; -7.9]
	Model	-19.0 [0 + 0 + 0 – 19.0]	-2.0 [0 – 2.0 + 0 – 0.1]	17.4 [15.3 + 0.3 - 0 + 1.8]	-16.4
WT, all inhibitors except amiloride	Microperfusion (n = 5)	-4.6 ± 2.3 [-10.9; 1.6]	-0.4 ± 1.4 [-4.4; 3.5]	14.2 ± 1.6 [9.7; 18.7]	-18.3 ± 4.7 [-31.4; -5.2]
	Model	- 2.2 [24.4 + 0 + 0 – 26.6]	6.7 [0 + 0.4 + 0 + 6.3]	9.7 [7.6 + 0.5 + 0 + 1.6]	-21.3
WT, Amiloride	Microperfusion (n = 5)	-32.7 ± 4.7 [-43.5; -21.9]	-7.8 ± 3.8 [-16.6; 0.9]	22.1 ± 1.5 [18.7; 25.5]	- 8.8 ± 2.2 [-14.0; -3.7]
	Model	-30.5 [0 – 14.9 +3.5 – 19.1]	-8.7 [0 – 16.6 + 7.0 + 0.9]	19.4 [11.8 + 6.1 + 0.1 + 1.4]	-16.9
HKA2$^{-/-}$, Amiloride	Microperfusion (n = 6)	-17.0 ± 1.5 [-20.9; -13.1]	-1.6 ± 2.1 [-7.1; 3.9]	20.6 ± 0.8 [18.6; 22.6]	- 9.0 ± 2.4 [-15.1; -2.8]
	Model	-16.3 [0 + 0 + 3.4 – 19.7]	2.4 [0 – 4.9 + 7.0 +0.3]	16.7 [15.4 – 0.7 + 0.2 + 1.8]	-16.0
WT, Amiloride + bumetanide	Microperfusion (n = 5)	- 18.4 ± 1.8 [-23.3 ; -13.4]	1.4 ± 1.8 [-3.5 ; 6.3]	18.4 ± 1.8 [13.4; 23.3]	- 13.0 ± 0.8 [-15.3; -10.6]
	Model	-23.1 [0 – 9.4 +3.5 – 17.2]	0.7 [0 – 4.4 + 7.0 – 1.9]	21.7 [11.7 + 8.4 + 0.1 + 1.4]	-16.3
WT, No inhibitors	Microperfusion (n = 14)	-8.2 ± 1.6 [-11.6; -4.7]	-1.3 ± 1.3 [-4.2; 1.6]	12.0 ± 0.9 [10.0; 14.0]	-20.2± 1.6 [-23.7; -16.8]
	Model	- 11.4 [+25.8 – 14.9 + 3.4 – 25.7]	3.1 [0 – 9.9 + 7.0 + 6.0]	12.3 [5.3 + 5.5 + 0.1 + 1.4]	-20.9

J_{Na}, J_{Cl}, J_K: transepithelial fluxes of Na^+, Cl^-, and K^+, in pmol/min/mm (positive flux values denote reabsorption, negative flux values denote secretion). ΔV_{te}: transepithelial electrical potential difference at the tubule inlet, in mV. Experimental values are given as mean ± s.e.m, followed by the 95% confidence interval. Model values denote predictions from the mathematical model. The overall flux is the sum of 4 components (shown within brackets), namely, the net fluxes across principal cells, type A and type B intercalated cells, and the paracellular pathway. “All inhibitors”: amiloride (10^{-5} M), HCTZ (10^{-4} M), and Schering 28080 (10^{-3} M) in the lumen, and bumetanide (10^{-4} M) in the bath.

Table 5

Model predictions under symmetric conditions

	J_{Na}	J_{Cl}	J_K	ΔV_{te}
Measured values	*+36.4 ± 3.3*	*+13.4 ± 2.0*	*-5.3 ± 1.0*	*-13.9 ± 2.6*
Predictions				
No adjustment	+ 24.3 [37.4 – 14.3 + 12.4 – 11.1]	3.0 [0 – 6.5 - 0.7 + 10.2]	- 6.0 [- 12.1 + 6.0 + 0.1 – 0]	- 9.1
NaCl TJ x 0.5	+ 26.6 [35.9 – 14.3 + 12.4 – 7.3]	+ 3.6 [0 – 2.6 -0.6 + 6.8]	- 7.7 [- 13.3 + 5.6 + 0.1 – 0.1]	- 11.8
NaCl TJ x 0.5 and ENaC x 1.25	+ 36.8 [48.0 – 14.2 +12.3 – 9.3]	+ 9.5 [0 + 1.6 -0.6 + 8.5]	- 11.8 [- 17.2 + 5.4 +0.1 – 0.1]	- 15.5
NaCl TJ x 0.5 and type A cell downregulation	+ 34.3 [34.4 – 4.0 +12.3 – 8.4]	+ 7.8 [0 + 0.8 -0.6 + 7.7]	- 10.8 [-12.3 + 1.4 +0.1 – 0.1]	-12.3
NaCl TJ x 0.5 and pendrin x 5	+ 30.0 [36.9 – 14.3 +15.0 – 7.6]	+ 10.8 [0 -2.5 + 6.5 + 6.8]	- 8.2 [-13.7 + 5.6 +0.1 – 0.2]	-12.0

J_{Na}, J_{Cl}, J_K: transepithelial fluxes of Na^+, Cl^-, and K^+, in pmol/min/mm. ΔV_{te}: transepithelial electrical potential difference at the tubule inlet, in mV. Measured values (in italics, mean ± s.e.m) are taken from Reference (Leviel *et al.*, 2010). Indicated within brackets are the 4 flux components (i.e., the net fluxes across principal cells, type A and type B intercalated cells, and the paracellular pathway). Model predictions assume varying scenarios: NaCl TJ x 0.5: the tight junction permeability to Na^+ and Cl^- is divided by 2; ENaC x 1.25: ENaC expression is multiplied by 1.25; pendrin x 5: pendrin expression is multiplied by 5; type A cell downregulation: the expression of HKA2, NKCC1 and apical Cl^- channels in type A cells is reduced by 75%.

FIGURE LEGENDS

Figure 1. Representation of principal and intercalated cells in mouse CCD. Shown are the main transcellular Na^+, K^+ and Cl^- transporters. The mathematical model accounts for the transport of water and 12 solutes along the full length of the tubule.

Figure 2. Measured transepithelial fluxes (in pmol/min/mm) of Na^+ (A), Cl^- (B), K^+ (C) and transepithelial voltage difference (D, in mV) in the CCDs of wild-type mice perfused under asymmetric conditions, in 3 cases: in the presence of amiloride, hydrochlorothiazide, bumetanide, and Schering 28080 ("paracellular"), in the presence of hydrochlorothiazide, bumetanide, and Schering 28080 ("paracellular + PC"), or in the presence of amiloride only ("paracellular + IC"). Results are shown as individual data and mean ± s.e.m.

Figure 3. Predicted fluxes across paracellular and transcellular pathways under asymmetric conditions, in the presence of amiloride, hydrochlorothiazide, bumetanide, and Schering 28080. Solute fluxes (in pmol/min/mm) are shown at the CCD inlet (panel A) and outlet (panel B), for a 1 mm-long tubule. Prescribed values (i.e., boundary conditions) are in italics. Not shown are basolateral Na^+/H^+ exchangers, basolateral $2Na^+$-HPO_4^{2-} cotransporters, and apical H^+/K^+-ATPase type 1 pumps.

Figure 4. Measured transepithelial fluxes (in pmol/min/mm) of Na^+ (A), Cl^- (B), K^+ (C) and transepithelial voltage difference (D, in mV) in the CCDs of wild-type mice perfused under asymmetric conditions, in the presence of amiloride only (WT) or in the presence of amiloride and bumetanide (WT+bumetanide), and in the CCDs of HKA2-null mice perfused under asymmetric conditions with amiloride (HKA2-KO). Results are shown as individual data and mean ± s.e.m.

Figure 5. Predicted fluxes (in pmol/min/mm) at the CCD inlet, under asymmetric conditions, with amiloride only (panel A) and with amiloride and bumetanide (panel B).

Not shown are basolateral Na^+/H^+ exchangers, basolateral $2Na^+$-HPO_4^{2-} cotransporters, and apical H^+/K^+-ATPase type 1 pumps.

Figure 6. Predicted fluxes (in pmol/min/mm) under asymmetric conditions, without inhibitors, at the CCD inlet (panel A) and outlet (panel B). Not shown are basolateral Na^+/H^+ exchangers, basolateral $2Na^+$-HPO_4^{2-} cotransporters, and apical H^+/K^+-ATPase type 1 pumps.

Figure 7. Measured (grey circles) and predicted (white circles) values of Na^+, Cl^-, K^+ fluxes (in pmol/min/mm) and of the transepithelial voltage difference (in mV) in the CCDs of wild-type mice perfused under asymmetric conditions, in the absence of inhibitors. Experimental results are shown as individual data and mean ± IC 95.

Figure 8. Daily Na^+ intake (A) and urinary Na^+ excretion (B) in WT (white bars) and HKA2-null mice (black bars) under normal conditions (control) and one day after switching to a high salt diet (3% NaCl in drinking water). Results are shown as mean ± s.e.m (n=5). * $p<0.05$.

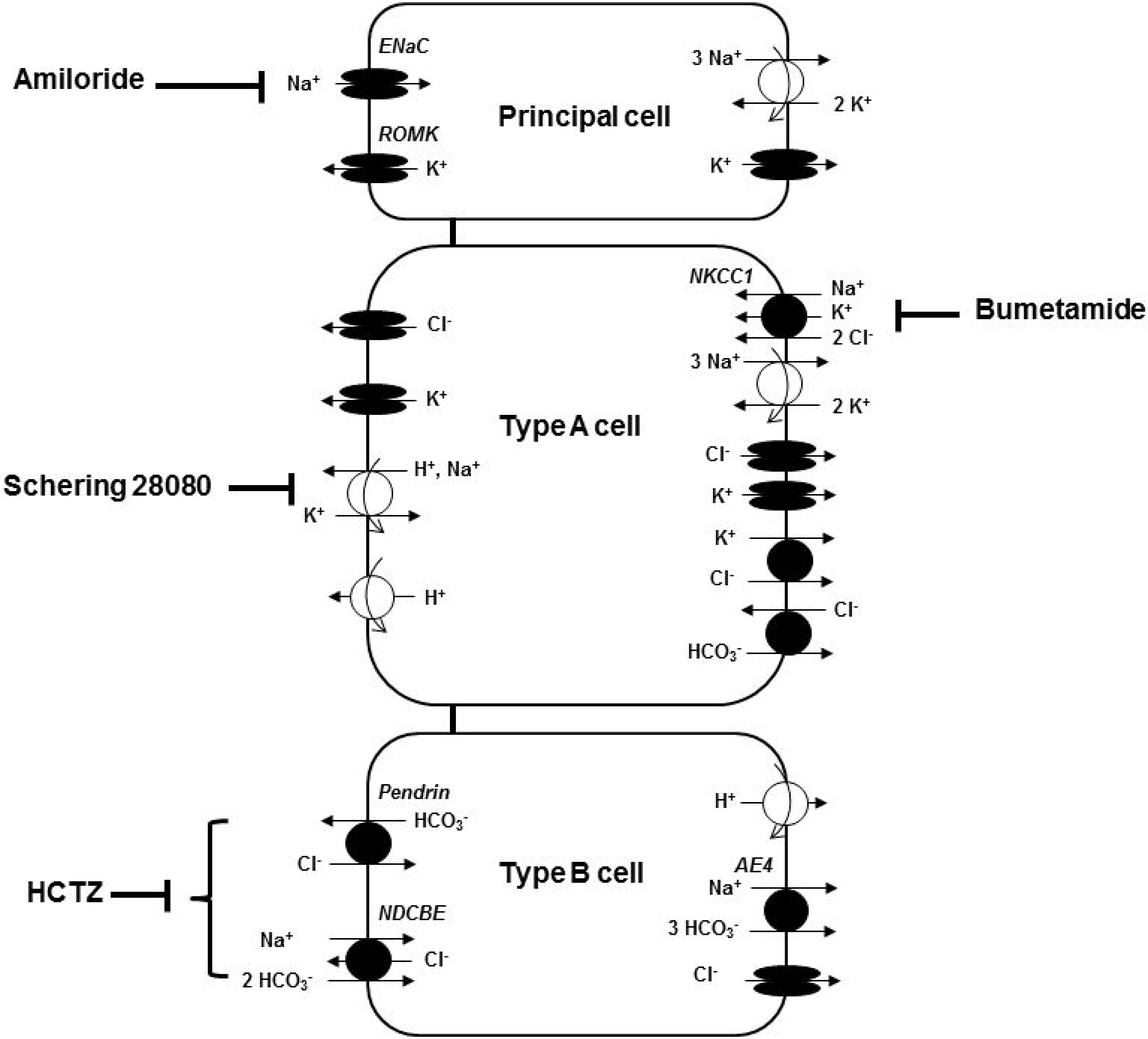
Amiloride
ENaC
Na^+
ROMK
K^+
Principal cell
3 Na^+
2 K^+
K^+
NKCC1
Na^+
K^+
2 Cl^-
Bumetamide
Cl^-
K^+
3 Na^+
2 K^+
Type A cell
Cl^-
K^+
Schering 28080
H^+, Na^+
K^+
K^+
Cl^-
H^+
Cl^-
HCO_3^-
Pendrin
HCO_3^-
Cl^-
H^+
Type B cell
AE4
Na^+
3 HCO_3^-
HCTZ
NDCBE
Na^+
Cl^-
2 HCO_3^-
Cl^-

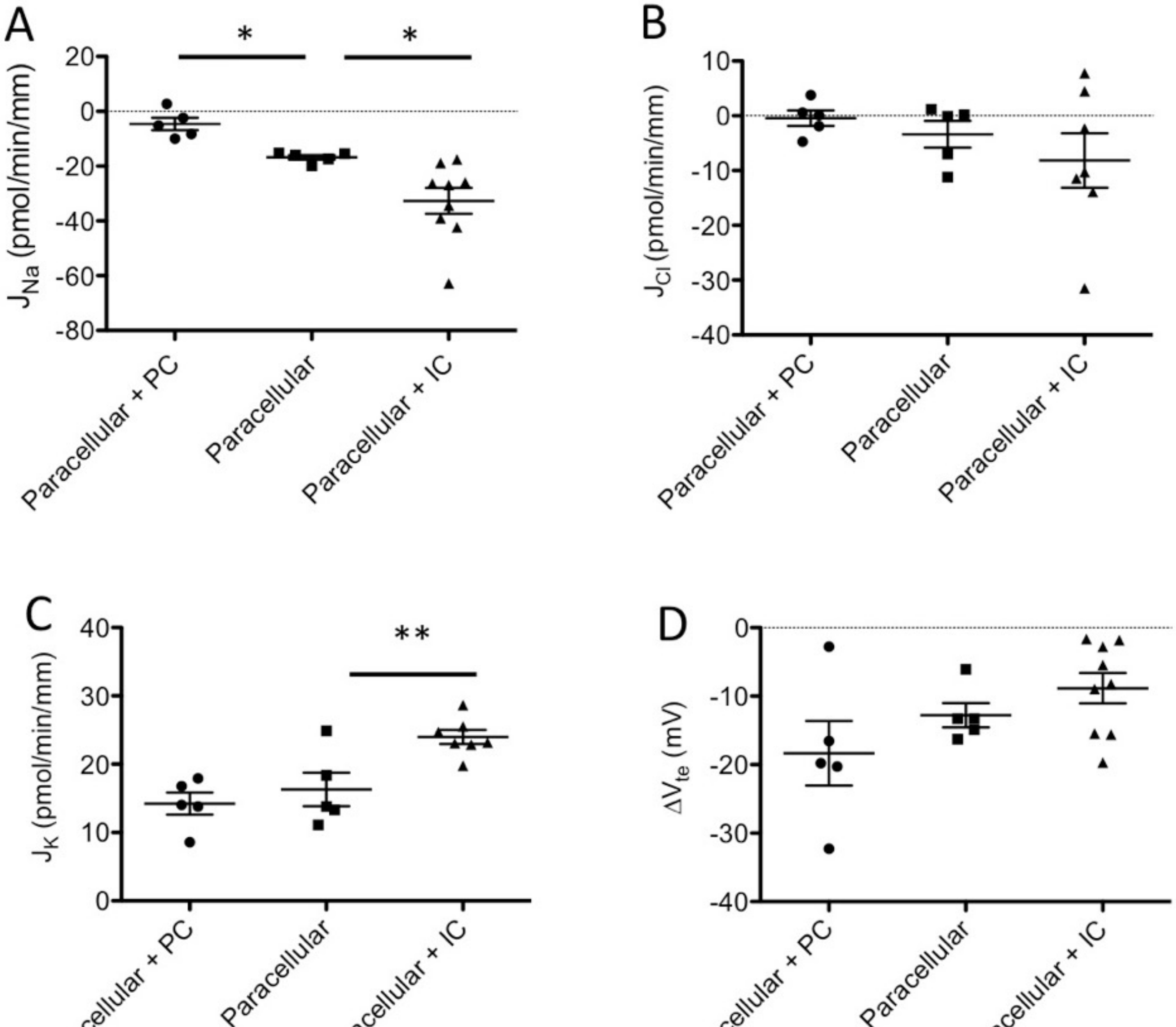
A
J_{Na} (pmol/min/mm)
20
0
-20
-40
-60
-80
*
*
Paracellular + PC
Paracellular
Paracellular + IC
B
J_{Cl} (pmol/min/mm)
10
0
-10
-20
-30
-40
Paracellular + PC
Paracellular
Paracellular + IC
C
J_K (pmol/min/mm)
40
30
20
10
0
**
Paracellular + PC
Paracellular
Paracellular + IC
D
ΔV_{te} (mV)
0
-10
-20
-30
-40
Paracellular + PC
Paracellular
Paracellular + IC

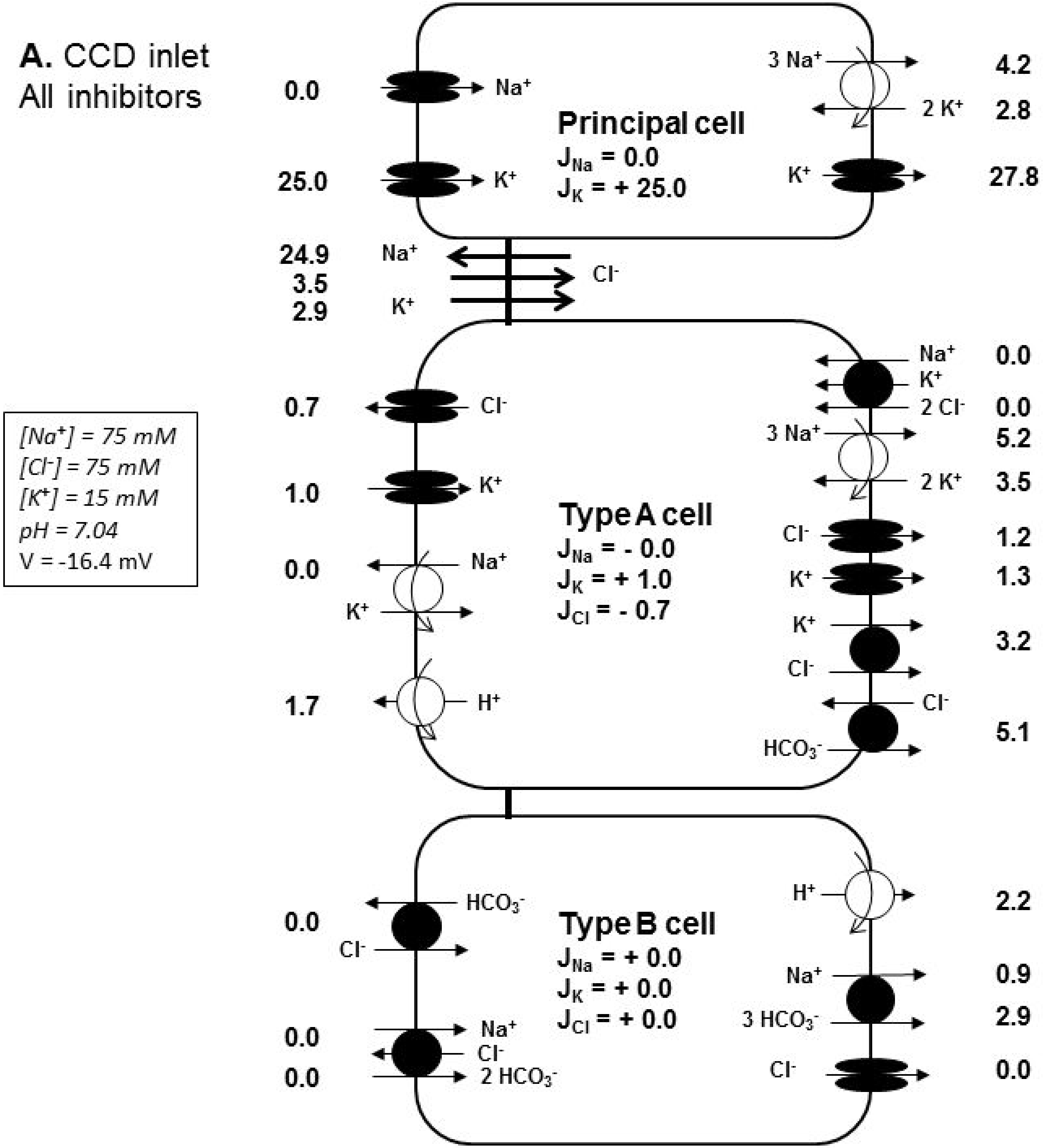

A. CCD inlet
All inhibitors
$[Na^+]$ = 75 mM
$[Cl^-]$ = 75 mM
$[K^+]$ = 15 mM
pH = 7.04
V = -16.4 mV
Principal cell
J_{Na} = 0.0
J_K = + 25.0
0.0 Na^+
25.0 K^+
$3\ Na^+$ 4.2
$2\ K^+$ 2.8
K^+ 27.8
24.9 Na^+
3.5 Cl^-
2.9 K^+
Type A cell
J_{Na} = - 0.0
J_K = + 1.0
J_{Cl} = - 0.7
0.7 Cl^-
1.0 K^+
0.0 Na^+ K^+
1.7 H^+
Na^+ K^+ 0.0
$2\ Cl^-$ 0.0
$3\ Na^+$ 5.2
$2\ K^+$ 3.5
Cl^- 1.2
K^+ 1.3
K^+ Cl^- 3.2
Cl^- HCO_3^- 5.1
Type B cell
J_{Na} = + 0.0
J_K = + 0.0
J_{Cl} = + 0.0
0.0 HCO_3^- Cl^-
0.0 Na^+
Cl^-
0.0 $2\ HCO_3^-$
H^+ 2.2
Na^+ 0.9
$3\ HCO_3^-$ 2.9
Cl^- 0.0

B. CCD outlet
All inhibitors

[Na^+] = 93 mM
[Cl^-] = 84 mM
[K^+] = 7 mM
pH = 6.60
V = -6.0 mV

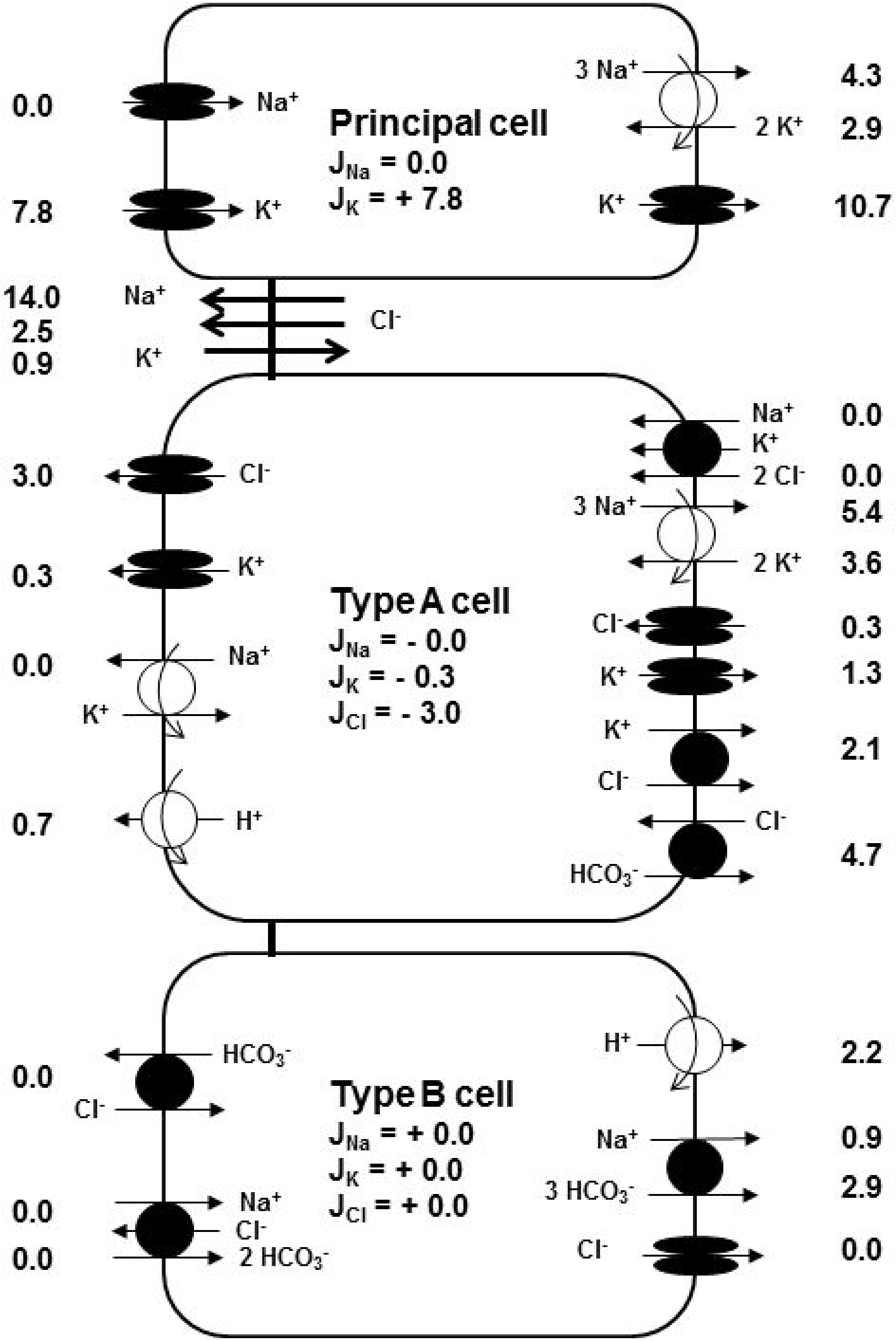
Principal cell
J_{Na} = 0.0
J_K = + 7.8
0.0
Na^+
7.8
K^+
3 Na^+
4.3
2 K^+
2.9
K^+
10.7
14.0
2.5
0.9
Na^+
Cl^-
K^+
Type A cell
J_{Na} = - 0.0
J_K = - 0.3
J_{Cl} = - 3.0
3.0
Cl^-
0.3
K^+
0.0
Na^+
K^+
0.7
H^+
Na^+
0.0
K^+
2 Cl^-
0.0
3 Na^+
5.4
2 K^+
3.6
Cl^-
0.3
K^+
1.3
K^+
Cl^-
2.1
Cl^-
HCO_3^-
4.7
Type B cell
J_{Na} = + 0.0
J_K = + 0.0
J_{Cl} = + 0.0
0.0
HCO_3^-
Cl^-
0.0
Na^+
Cl^-
0.0
2 HCO_3^-
H^+
2.2
Na^+
0.9
3 HCO_3^-
2.9
Cl^-
0.0

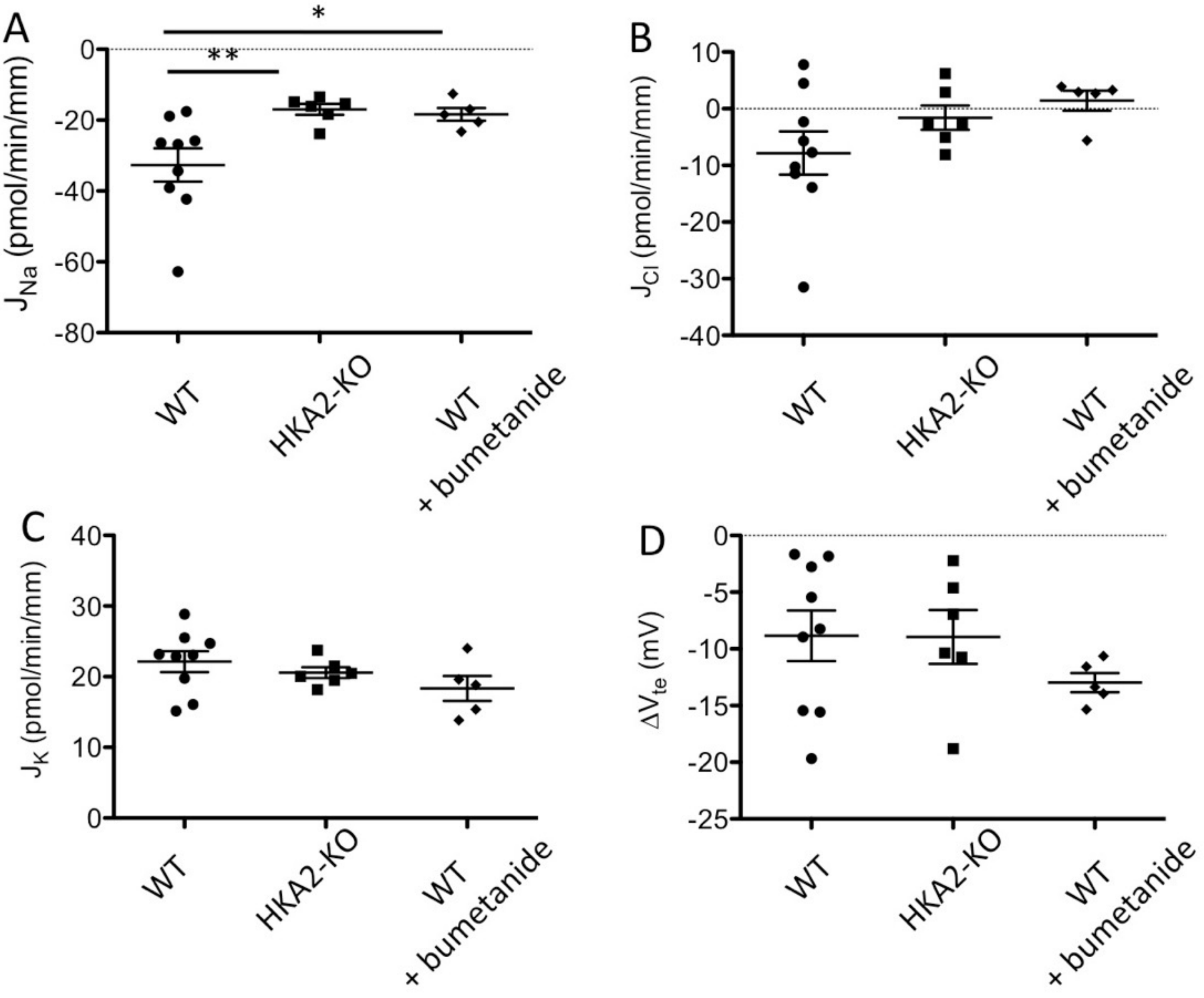
A
J_{Na} (pmol/min/mm)
0
-20
-40
-60
-80
*
**
WT
HKA2-KO
WT + bumetanide
B
J_{Cl} (pmol/min/mm)
10
0
-10
-20
-30
-40
WT
HKA2-KO
WT + bumetanide
C
J_K (pmol/min/mm)
40
30
20
10
0
WT
HKA2-KO
WT + bumetanide
D
ΔV_{te} (mV)
0
-5
-10
-15
-20
-25
WT
HKA2-KO
WT + bumetanide

A. CCD inlet
With amiloride

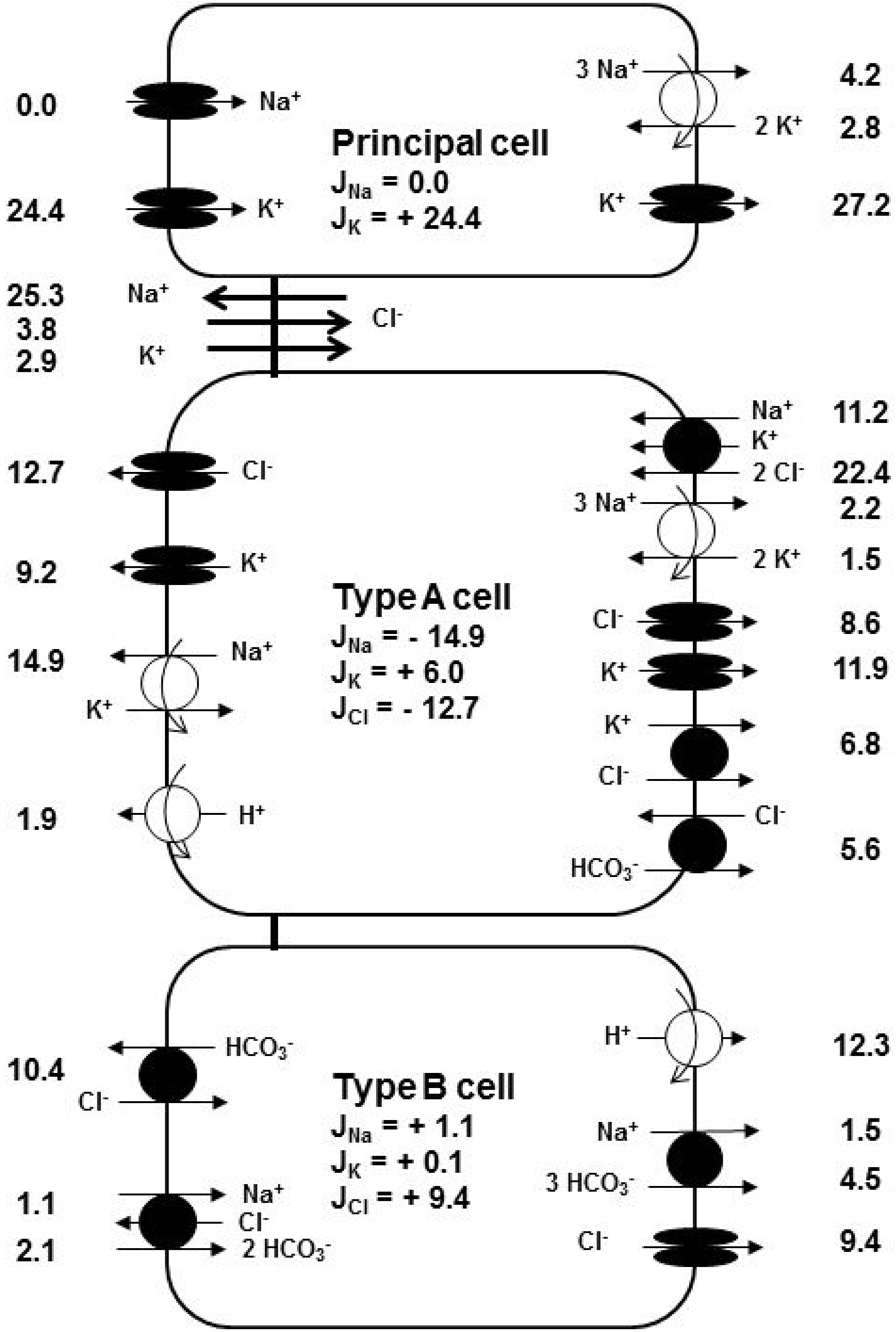
0.0
Na⁺
24.4
K⁺
Principal cell
J_Na = 0.0
J_K = + 24.4
3 Na⁺
4.2
2 K⁺
2.8
K⁺
27.2
25.3
Na⁺
3.8
Cl⁻
2.9
K⁺
Type A cell
J_Na = - 14.9
J_K = + 6.0
J_Cl = - 12.7
12.7
Cl⁻
9.2
K⁺
14.9
Na⁺
K⁺
1.9
H⁺
Na⁺
11.2
K⁺
2 Cl⁻
22.4
3 Na⁺
2.2
2 K⁺
1.5
Cl⁻
8.6
K⁺
11.9
K⁺
Cl⁻
6.8
Cl⁻
HCO₃⁻
5.6
Type B cell
J_Na = + 1.1
J_K = + 0.1
J_Cl = + 9.4
10.4
HCO₃⁻
Cl⁻
1.1
Na⁺
Cl⁻
2.1
2 HCO₃⁻
H⁺
12.3
Na⁺
1.5
3 HCO₃⁻
4.5
Cl⁻
9.4

[Na$^+$] = 75 mM
[Cl$^-$] = 75 mM
[K$^+$] = 15 mM
pH = 7.04
V = -16.9 mV

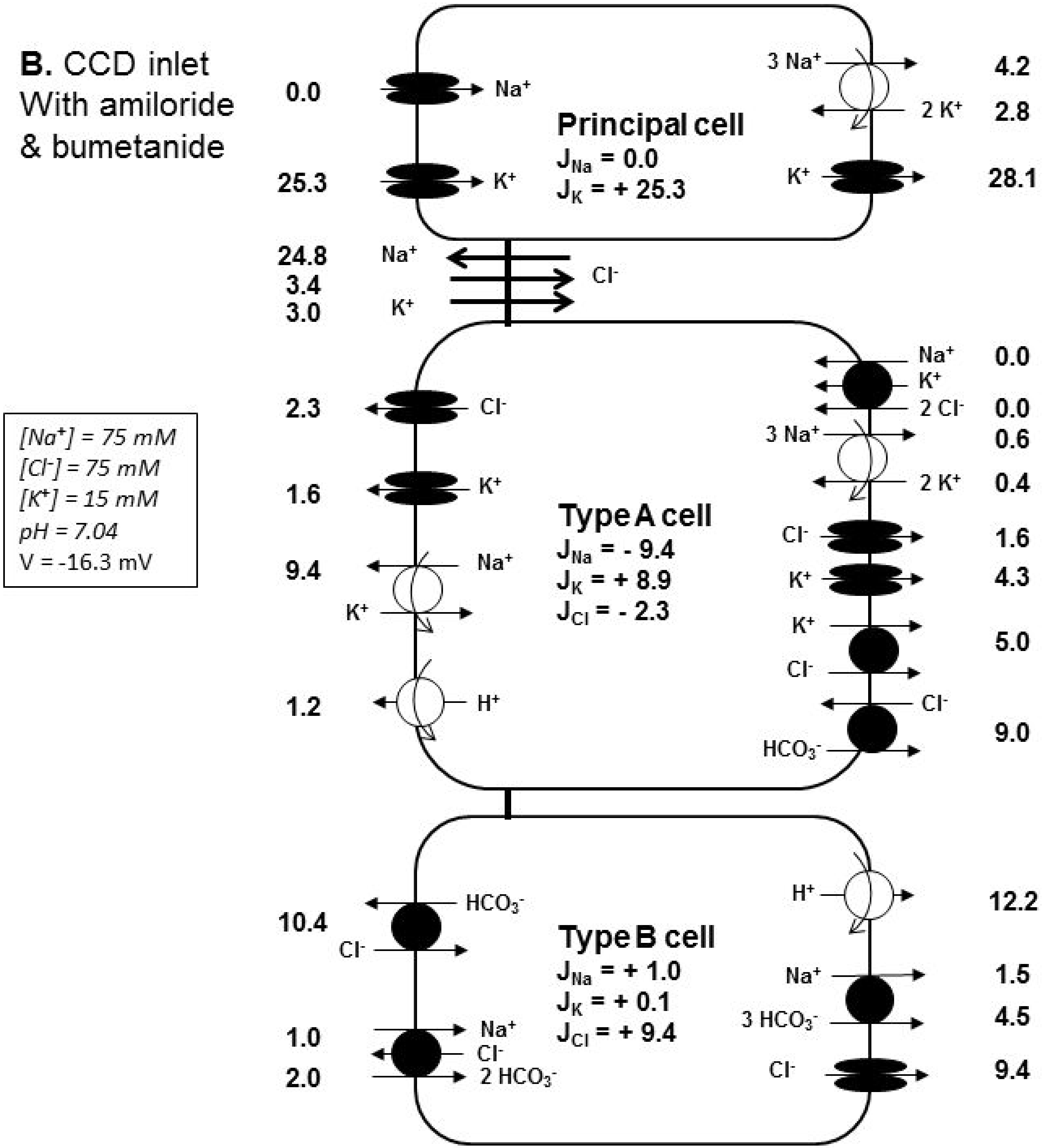
B. CCD inlet
With amiloride
& bumetanide
$[Na^+]$ = 75 mM
$[Cl^-]$ = 75 mM
$[K^+]$ = 15 mM
pH = 7.04
V = -16.3 mV
Principal cell
J_{Na} = 0.0
J_K = + 25.3
0.0
Na^+
25.3
K^+
3 Na^+
4.2
2 K^+
2.8
K^+
28.1
24.8
Na^+
3.4
Cl^-
3.0
K^+
Type A cell
J_{Na} = - 9.4
J_K = + 8.9
J_{Cl} = - 2.3
2.3
Cl^-
1.6
K^+
9.4
Na^+
K^+
1.2
H^+
Na^+
0.0
K^+
2 Cl^-
0.0
3 Na^+
0.6
2 K^+
0.4
Cl^-
1.6
K^+
4.3
K^+
Cl^-
5.0
Cl^-
HCO_3^-
9.0
Type B cell
J_{Na} = + 1.0
J_K = + 0.1
J_{Cl} = + 9.4
HCO_3^-
10.4
Cl^-
1.0
Na^+
Cl^-
2.0
2 HCO_3^-
H^+
12.2
Na^+
1.5
3 HCO_3^-
4.5
Cl^-
9.4

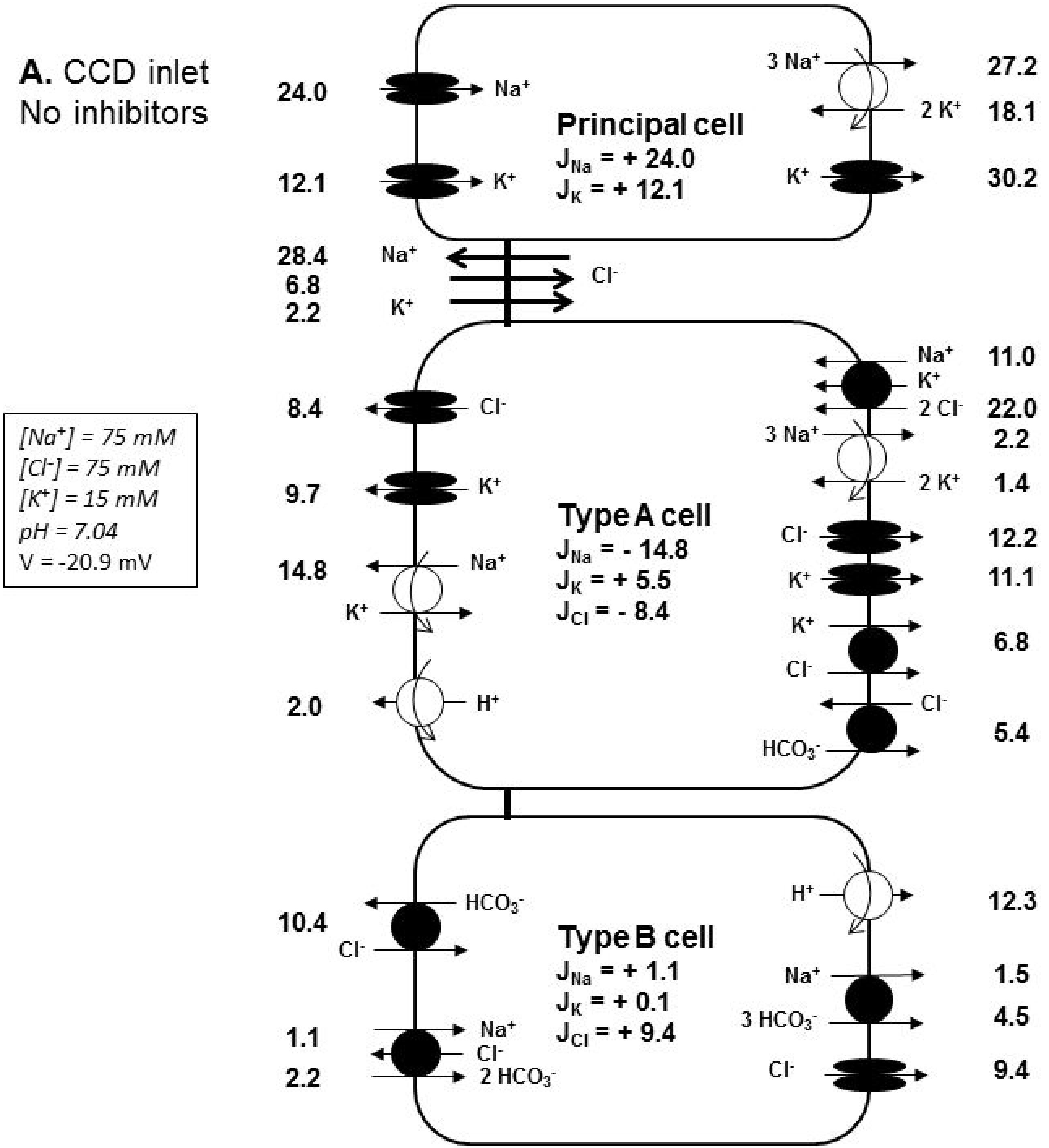
A. CCD inlet
No inhibitors
[Na+] = 75 mM
[Cl-] = 75 mM
[K+] = 15 mM
pH = 7.04
V = -20.9 mV
Principal cell
J_Na = + 24.0
J_K = + 12.1
24.0
Na+
12.1
K+
3 Na+
27.2
2 K+
18.1
K+
30.2
28.4
Na+
6.8
Cl-
2.2
K+
Type A cell
J_Na = - 14.8
J_K = + 5.5
J_Cl = - 8.4
8.4
Cl-
9.7
K+
14.8
Na+
K+
2.0
H+
Na+
11.0
K+
2 Cl-
22.0
3 Na+
2.2
2 K+
1.4
Cl-
12.2
K+
11.1
K+
Cl-
6.8
Cl-
HCO3-
5.4
Type B cell
J_Na = + 1.1
J_K = + 0.1
J_Cl = + 9.4
HCO3-
10.4
Cl-
1.1
Na+
Cl-
2.2
2 HCO3-
H+
12.3
Na+
1.5
3 HCO3-
4.5
Cl-
9.4

B. CCD outlet
No inhibitors

$[Na^+]$ = 89 mM
$[Cl^-]$ = 82 mM
$[K^+]$ = 10 mM
pH = 6.43
V = -16.9 mV

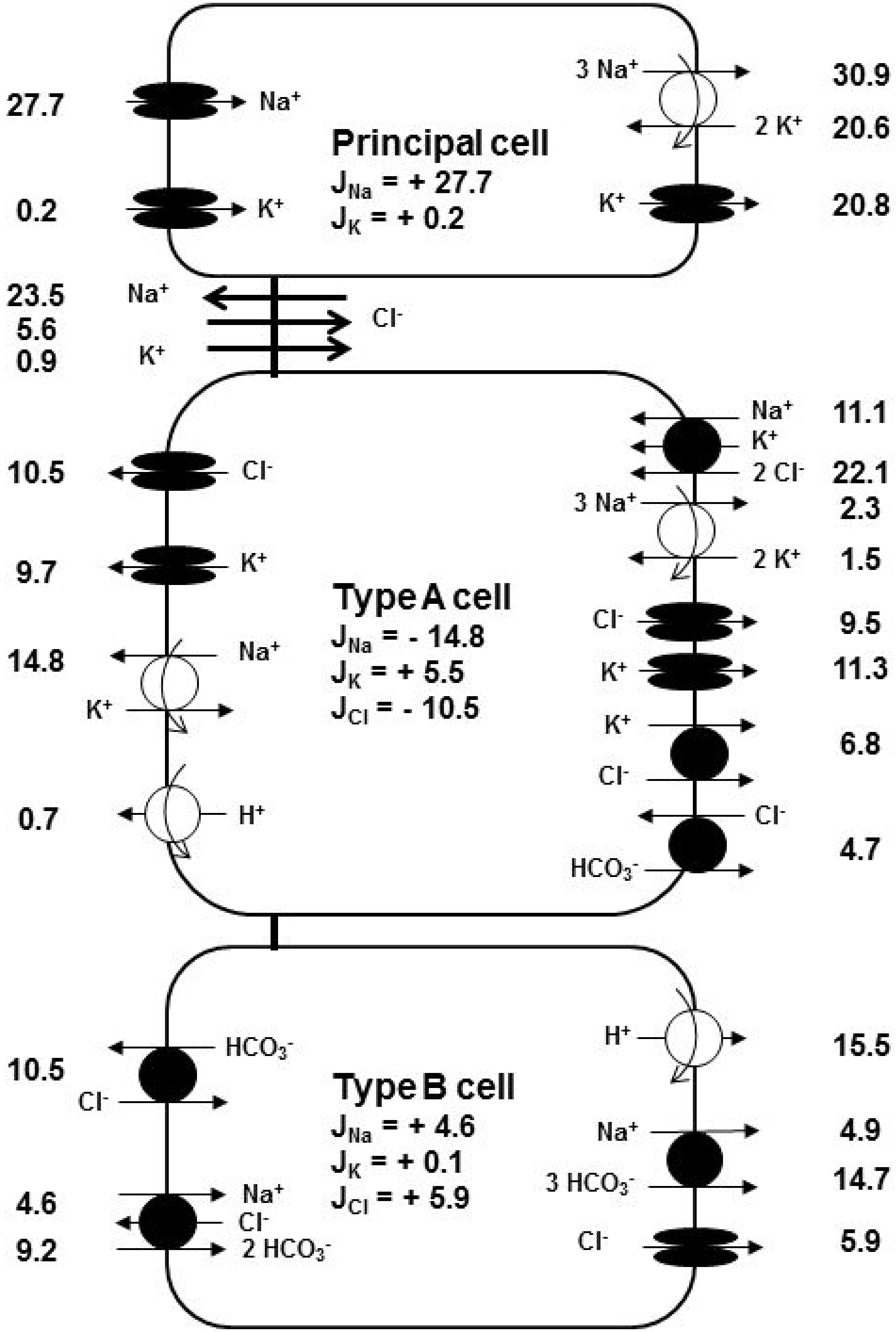

27.7
Na^+
3 Na^+
30.9
2 K^+
20.6
Principal cell
J_{Na} = + 27.7
J_K = + 0.2
0.2
K^+
K^+
20.8
23.5
Na^+
5.6
Cl^-
0.9
K^+
Na^+
11.1
K^+
2 Cl^-
22.1
10.5
Cl^-
3 Na^+
2.3
2 K^+
1.5
9.7
K^+
Type A cell
J_{Na} = - 14.8
J_K = + 5.5
J_{Cl} = - 10.5
Cl^-
9.5
14.8
Na^+
K^+
11.3
K^+
K^+
6.8
Cl^-
0.7
H^+
Cl^-
4.7
HCO_3^-
H^+
15.5
10.5
HCO_3^-
Cl^-
Type B cell
J_{Na} = + 4.6
J_K = + 0.1
J_{Cl} = + 5.9
Na^+
4.9
3 HCO_3^-
14.7
4.6
Na^+
Cl^-
9.2
2 HCO_3^-
Cl^-
5.9

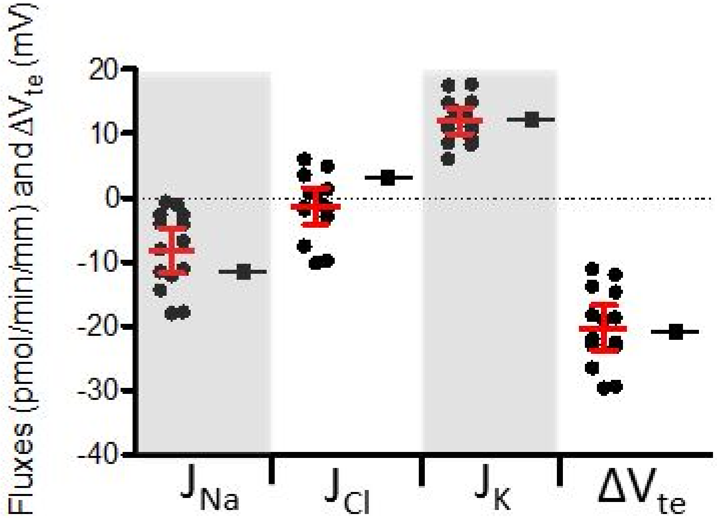
Fluxes (pmol/min/mm) and ΔV_te (mV)
20
10
0
-10
-20
-30
-40
J_Na
J_Cl
J_K
ΔV_te

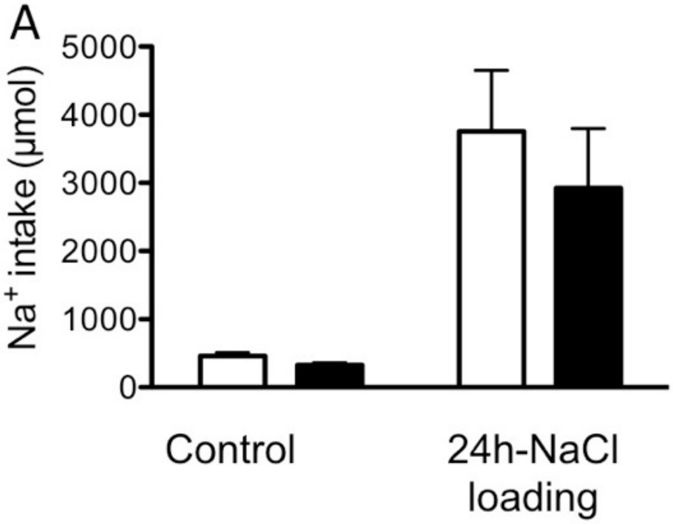
A
Na⁺ intake (µmol)
5000
4000
3000
2000
1000
0
Control
24h-NaCl loading

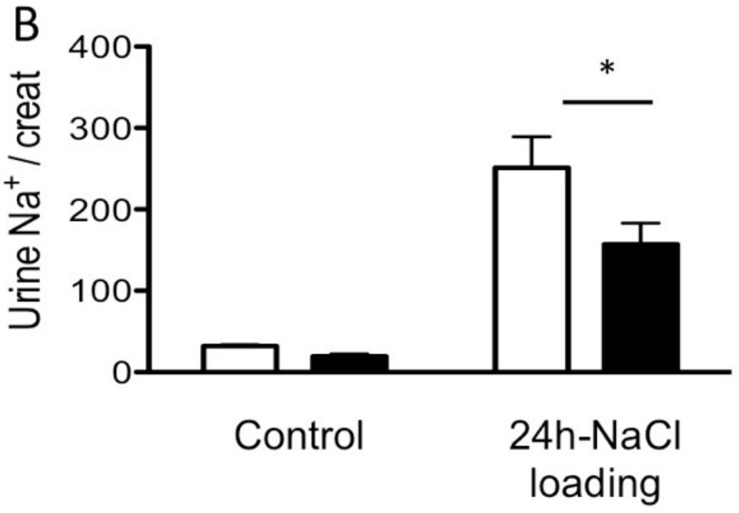
B
Urine Na⁺ / creat
400
300
200
100
0
*
Control
24h-NaCl loading